Modelling and robust estimation of AV node function during AF

Luca Iozzia, Gennaro Garoldi

2014

LUND UNIVERSITY

Master's Thesis

Electrical measurements

Faculty of Engineering, LTH
Department of Biomedical Engineering

Supervisor: Frida Sandberg

Contents

Abstract

Objective: The purpose of the present thesis is to enrich the robustness of a statistical atrioventricular (AV) node model during atrial Fibrillation (AF). The model takes into account electrophysiological properties as the two pathways, their refractory periods and concealed conduction; these pathways are located between sinoatrial (SA) and AV node. It is highly desirable understanding of the AV node function, in order to achieve optimal arrhythmia management for those patients affected by AF, which is the most common arrhythmia. ***Methods***: The simulation has been improved by introducing a new parameter that represents the probability of an impulse choosing either one of the two pathways. Exploration data has been conducted keeping fixed a set of parameters while varying one of them. ***Results***: The model concerns a relationship between the probability of an atrial impulse passing through (output parameter, α) and choosing (input parameter, γ) either one of two pathway. To test its accuracy and precision mean absolute error (MAE) and root mean square error (RMSE) have been calculated for different γ, obtaining, $MAE = 3.8 \pm 8.2023 * 10^{-4}$ and $RMSE = 1.59 \pm 0.87 * 10^{-2}$. Moreover, an investigation has been conducted on real data to verify the proposed relationship using estimated parameter made by the previous model. Dataset consists 24-h Holter recordings on 31 patients, for each patient there is a baseline and 4 different treatments recordings. The results showed that the standard deviation of introduced parameter presents a greater stability in 58% of recordings, and t-test has given a not significant difference. ***Conclusion:*** This study indicates that the proposed relationship can be used to calculate the input parameter γ, given estimated parameter α. However, it is necessary to develop a new estimation model using the actual RR-series interval simulation.

Index terms: Atrial Fibrillation (AF), atrioventricular node (AV node), Carvedilol, Diltiazem, dual pathways, Holter recordings, maximum likelihood estimation (MLE), minimum least squares (MLS), metoprolol, refractory period, RR intervals, statistical modeling, Verapamil.

List of acronyms

Action Potential, AP
Adenosine triphosphate, ATP
Atrial Fibrilaton, AF
Atrial Impulse, AI
Atrioventricular node, AV node
Effective Refractory Period, ERP
Electrocardiography, ECG
Direct Current, DC
Joint Probability Function, JPF
Maximum Likelihood Estimation algorithm, MLE algorithm
Mean Absolute Error, MAE
Minimum Least Square algorithm, MLS algorithm
Probability Density Function, PDF
RATe control during Atrial Fibrillation, RATAF
Root Mean Square Error, RMSE
Simulated Annealing, SA
Sinoatrial node, SA node

Chapter 1

Introduction

Atrial fibrillation (AF) is the most common arrhythmia [1]. During AF the normal regular electrical impulses generated by the sinoatrial node (SA node) are compromised, bearing disorganized electrical impulses (400-700 beats/minute), and leading to irregular conduction of ventricles impulses, usually with a ventricular rate at 140-220 beats/minute. AF is often associated with palpitations, fainting, chest pain, stroke, or congestive heart failure, other hand it may cause no symptoms. The most important risk is associated to stroke, which is caused primarily by cloths forming in the atria.
The rise in the prevalence of AF can be predominantly attributed to ageing of the population and to a higher incidence of cardiovascular diseases. The first symptom of arrhythmia can be verified by taking the pulse, while the diagnosis and classification of AF is provided by electrocardiogram (ECG) where it is feasible to notice the presence of AF-events, like absence of P waves and irregular ventricular rate. The AF classification can be divided in paroxysmal, persistent and permanent.

During AF the AV node plays a relevant role in order to block many of atrial impulses that arrive according to an irregular and chaotic activity. Although the electrophysiological properties of the AV node influence the ventricular response during AF, they are not routinely evaluated in clinical practice. Therefore, different mathematical models have been proposed, both invasive and non-invasive to better understand the AV node behaviour, e.g. Cohen model [2] and Lian model [3].
The present thesis is based on a previous work made by Corino et *al.*[4] whose aim has been to develop an estimation model of the AV node during the AF, applied on ECG signal. By the ECG, the generation of RR intervals histogram is obtained, thanks to which the estimation of parameters of the model is developed using maximum likelihood method. These parameters takes into account the general electrophysiological properties of the conduction system: (1) presence of dual AV nodal pathways; (2) relative refractory

periods of the pathways; (3) prolongation time due to the concealed conduction phenomenon. However the result, applied on real data, presents a high variability in the estimated parameters.
Starting from this point, the purpose of the thesis is to enrich the robustness of the model, by the introduction of a new parameter that is more correlated to the physiological characteristics of AV node. The final expected result is the relationship between the new parameter and the parameters estimated by the previous model. The ECG signals, on which the evaluation of the results has been done, are taken from the RATAF database where it was recorded a 24-hour Holter ECG for each patient affected by AF. The registrations have been achieved for each of the four drugs administration (Metoprolol, Verapamil, Carvedilol and Diltiazem) and one recording without.

The first part of the thesis, Ch. 2, contains the medical background useful to be introduced in the argument of the cardiac conduction system. In Sec 2.5 the attention is focused on the pathophysiology of the AF including diagnosis, classification and treatment. Afterwards there is an overall explanation of the AV node anatomy on which the thesis is based on. In the next Ch. 3 the description of the main algorithms used in the model (MLE, simulated annealing and generalized pattern search) is conducted, as well as the theory of Poisson process and the Lambert function. The second part of the thesis contains the description of the adopted method, Ch. 4. After a brief introduction of some previous mathematical models, including the implementation Corino model, schematic representation of the modified model is present. The Ch. 5 takes into account the results obtained in the simulation, Sec 5.1, and in the real data, Sec 5.2, applying the new model. Finally the Ch. 6 and 7 contain encountered problems, remarks, suggestions for future work and conclusion.

Chapter 2

Medical Background

In the following chapter a general description of the cardiac anatomy and physiology is described. In the next sections the reader is introduced to the cardiac conduction system, focusing the attention on the pathology of AF and its effects on the AV node.

2.1 Cardiac Anatomy and Physiology

The heart couches in the center of the thoracic cavity and is hanging by its attachment to the great vessels within a fibrous sac known as the pericardium. It is possible to consider the heart as "double pump": the gross anatomy of the right heart pump is considerably different from that of the left heart pump, performing their function in different districts, yet the pumping principles of each are primarily the same.[5]

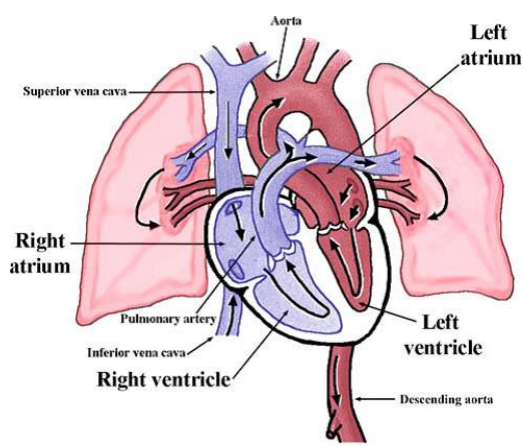

Fig. 2.1: Pathway of blood flows through the heart and lungs [5].

The heart is composed by four chambers, the two upper chambers are

the atria while the remaining lower are ventricles. The ventricles are closed chambers surrounded by muscular walls, and the valves, that separate them from the atria, are structurally designed to allow flow in only one direction, i.e. , from the atria to the ventricles. The cardiac valves passively open and close in response to the direction flow according to the pressure gradient across them. The function of the heart is to pump oxygenated and de-oxygenated blood at fixed ratio and pressure values, according to body requests and so keeping homeostasis which is the ability or tendency to maintain internal stability in an organism to compensate for environmental changes. Describing the pathway of blood, it flows through the chambers of the heart, as it is indicated in Fig. 2.1. The venous blood returns from the systemic organs to the right atrium via the superior and inferior venae cavae. Then it passes through the tricuspid valve into the right ventricles and from there it is pumped through the pulmonary valve into the pulmonary artery. After passing through the pulmonary capillaries, the oxygenated pulmonary venous blood returns to the left atrium through the pulmonary veins. The flow of blood then passes through the mitral valve into the left ventricle and is pumped through the aortic valve into the aorta. After that it begins the systemic blood circulation [5]. During the circulation, venous and arterial blood does not mix, indeed it flows in two separated vessels. The gas exchange happens at the level of the capillary vessels and alveoli pulmonary, under particular conditions of partial pressure of P_{O_2}. This phenomenon is due to haemoglobin structure [6]. Observing the saturation of haemoglobin curve, in Fig. 2.2, it is comprehensible how it works in different part of the human body, releasing or linking O_2 molecules. Indeed, those areas with high P_{O_2} value can be categorizd as pulmonary alveoli where the haemoglobin links with O_2 molecules. Viceversa, areas with a low value correspond to those organs where haemoglobin releases oxygen.

The cardiac anatomy is composed mainly by muscle cells (myocytes), see Fig. 2.3. Muscle cells are similar to the other somatic cells (they contain common organelles) but distinct as they also include an elaborate protein scaffold that is anchored to the cell membrane. Force generation by proteins within the matrix leads to the contraction of the cells and pumping of blood by the heart. Force is produced primarily along the long axis of the cell. Most of the internal volume of myocytes is devoted to a cytoskeletal lattice of contractile proteins whose liquid crystalline order gives rise to a striated appearance under the microscope. As with other cell types, the bilayer membrane contains a collection of ion channels and ion pumps and receptor proteins. In addition, the membranes of cardiac muscle cells contain proteins designed to connect

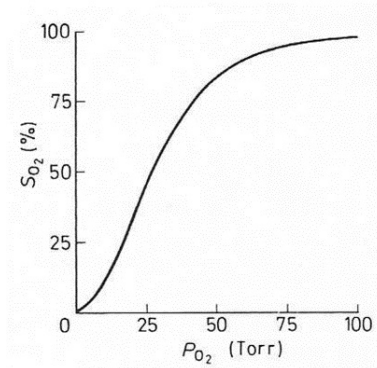

Fig. 2.2: Haemoglobin dissociation curve [6]. Torr is non-SI unit equal to [mmHg]

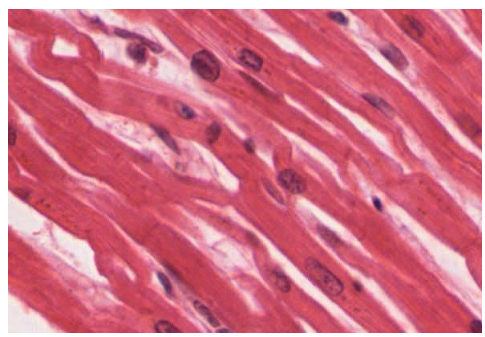

Fig. 2.3: Examples of myocyte cells obtained from microscope [7].

cardiac myocytes to one another as both mechanical and electrical partners.

2.2 The cardiac conduction system

The effective pump-action of the heart requires a precise coordination of the myocardial contractions and signal generation action potential (AP). This is accomplished via the cardiac conduction system, see Fig. 2.4. Contractions of each cell are normally started when electrical excitatory impulses generate along their surface membranes. In the healthy heart, the normal site for initiation of a heartbeat is within the "sinoatrial node" (SA node). The SA node is located in the right atrium in the heart and serves as the natural pacemaker. These pacemaker cells manifest natural depolarizations and are thus responsible for initiating the normal cardiac rhythm. Here specialized muscle cells have a membrane oscillator, which always spontaneously generates repetitive APs.

The electrical activity of these cells is characterized by a slow depolarization of the membrane potential (mV), the pacemaker potential, which is responsible for triggering each AP. The steepness of this pacemaker potential defines the frequency of the cardiac rhythm. This rhythmic activity is related to the interplay between a number of channels and the Na^{+}/Ca^{++} exchanger. The main currents beard by these different components can be divided into two groups, depending on whether they contribute to the pacemaker or the AP.
After initial SA nodal excitation, depolarization spreads throughout the atria. It is generally accepted that: (1) the spread of depolarizations from nodal cells can go directly to adjacent myocardial cells;(2) preferentially ordered myofibril pathways allow this excitation to rapidly traverse the right atrium to both the left atrium and the AV node. It is believed that there are three preferential anatomic conduction pathways from the SA node to the AV node [2]. These pathways are microscopically identifiable structures, appearing to be preferentially oriented fibres that provide a direct node-to-node pathway.
More specifically, the anterior tract is described as extension from the front

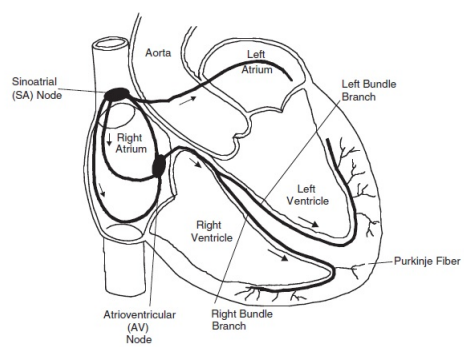

Fig. 2.4: General geometric conduction system [8].

part of the sinoatrial node, dividing into the so called Bachman's bundle (bearing impulses to the left atrium) and a second tract that dips along the interatrial septum which unites to the anterior part of the AV node. The middle (or Wenckebach's) pathway boosts from the superior part of the SA node, passes posteriorly to the superior vena cava, then unites the anterior bundle as it enters the AV node. The third pathway is defined as being posterior (Thorel's) which is considered to extend from the inferior part of the SA node, passing through the crista terminalis and the Eustachian valve nearby the coronary sinus to enter the posterior portion of the AV node [9], see Fig. 2.14 and section 2.6 for more details. At the ending of atrial depolarization, the excitatory signal reaches the AV node. This excitation arrives to

these cells via the aforementioned atrial ways, with the final excitation of the AV node generally described as occurring via the slow or fast pathways, see section 2.6.1. Following AV nodal excitation, in normal condition, the slow pathway conducts impulses to the "His bundle", indicated by a longer interval between atrial and His activation (note that the bundle of His has also been referred to as the "common bundle"). After leaving the bundle of His, the normal wave of cardiac depolarization spreads to both the left and right bundle branches; these pathways lead depolarization to the left and right ventricles, respectively. Finally, the signal essentially travels through the remnant of the Purkinje fibers and the ventricular myocardial depolarization spreads.

2.3 Channel cell mechanisms (action potential generation)

The contraction mechanism is spread out to the others cardiac muscle cells by AP. Their electrical activity is fundamental to have a normal function and due to the properties of the cell membrane takes advantage of to selectively pass charged species from inside to outside and vice versa. Most cells build a charge gradient using the action of ion pumps, ion selective channels and Adenosine Trio-Phosphate-dependent ion pumps (ATP-dependent ion pumps). The charge difference across a membrane creates an electrical potential, defined as the resting membrane potential of the cell. In the resting state, the inner part of the cell carries a negative charge relative to the exterior interstitial environment. The energy connected through the discharging of this potential is usually coupled with cellular functions. In excitable cells, temporally changes in the electrical potential (so the APs is like a "bolus" that goes through nervous system) are used to either communicate or to work. Importantly, in the myocyte, AP is required to initiate the process known as excitation contraction coupling. The extracellular fluid has an ionic composition similar to that of blood serum. The total intracellular concentration of calcium is higher, but much of it is bound to proteins or sequestered in organelles (mitochondria, sarcoplasmic reticulum). Hence, free myoplasmic concentrations are very low and expose in the micro-molar range in Tab. 2.1. ATP-dependend ion pumps, ion-specific channel proteins , and ion exchange proteins are all required to maintain the potential difference in ion concentrations. This separation of charged species across a resistive barrier (the cell membrane) generates the electrical potential (E_{ion}) mentioned above. For each ionic species, the value of this potential can be calculated using the Nernst equation [10]:

Ion	Inside (mM)	Outside (mM)	Ratio of inside/outside	E_{Eion*}* (mV)
Sodium	15	14	9.7	+60
Potassium	150	4	0.027	-94
Chloride	5	120	24	-83
Calcium	10^{-7}	2	$2x10^4$	+129

Tab. 2.1: Major ionic species contributing to the resting potential of cardiac muscle cells [5]

$$E_{ion} = -\frac{RT}{zF} ln \frac{[outside]}{[inside]} \tag{2.1}$$

where R is the gas constant, T is the temperature expressed in K degrees, z is the valence of the ion (charge and magnitude), and F is the Faraday constant. The membrane potentials of living cells depend not only of the potassium distribution, but also on diverse parameters including the concentrations of the other major ion species on both sides of the membrane as well as their relative permeabilities. To determine the overall membrane potential (E_m), a modified Goldman−Hodkin−Katz equation [11] is used to take into account the equilibrium potentials for individual ions and the permeability (conductance) of the membrane for each species such that

$$E_m = \frac{g_N a}{g_{tot}} E_{Na} + \frac{g_K}{g_{tot}} E_K + \frac{g_{Ca}}{g_{tot}} E_{Ca} \tag{2.2}$$

where g_{Na} is the membrane conductance for sodium (Na), g_K is the membrane conductance for potassium (K), g_{Ca} is the membrane conductance for calcium (Ca), g_{tot} is the total membrane conductance, E_{Na} is the equilibrium potential for sodium, E_K is the equilibrium potential for potassium, and E_{Ca} is the equilibrium potential for calcium. Evaluation of 2.2 equation using the values in 2.1 and the conductance values for sodium, potassium, and calcium results in a membrane potential of -90 mV.

The various phases of the cardiac AP, see Fig. 2.5, are associated with changes in the flow of ionic currents across the cell membrane. Atrial and ventricular cardiac muscle cells have an extremely rapid initial transition from the resting membrane potential to depolarization. Deepening as the channels allow charge movements, the AP generation is composed by five phases:

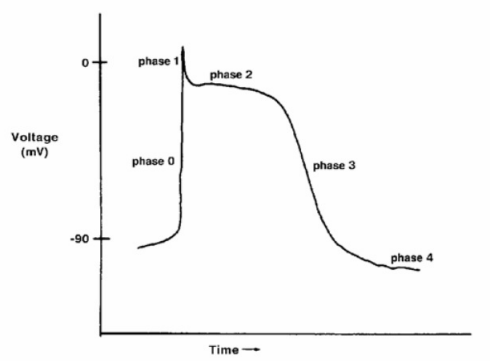

Fig. 2.5: The cardiac action potential [12].

phase 0
: As the sodium channels begin to close, the Na-channels open and there is a large-amplitude, short-duration inward Na-current.

phase 1
: It is defined as a small initial re-polarization. The opening of the L-type calcium channels causes a calcium influx and is balanced by the potassium efflux via the now open K-channels.

phase 2
: This balance results in the electrically positive plateau of the cardiac AP profile.

phase 3
: As the Ca-channels close, the flux of ions through the K-channels begins to dominate the membrane potential and re-polarization of the cells begins.

phase 4
: It represent the restoration of the resting membrane potential and the closing of the K-channels.

From the initiation of the AP through approximately half of the re-polarization, the cell is considered **refractory**, meaning that it could not respond to a new depolarization signal.

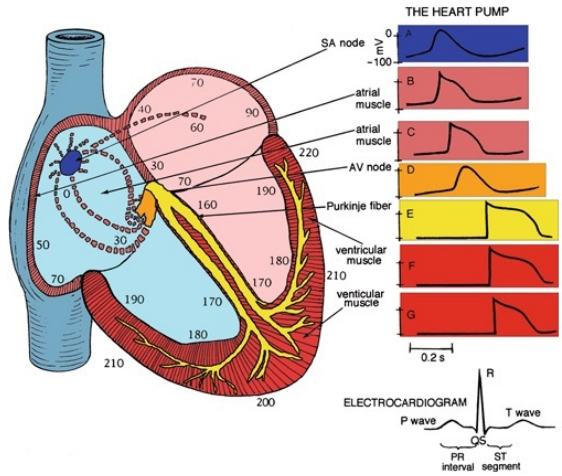

Fig. 2.6: APs develops long the cardiac conduction system. All these contributes are visible on the ECG as P wave, QRS complex and T wave, the QRST wave [5].

2.4 Electrocardiography

The most common cardiac investigation method is the electrocardiography (ECG). An ECG describes the electrical activity of the heart recorded by electrodes (leads) placed on the body surface. The voltage variations measured by the electrodes are caused by the APs of the excitable myocytes as they make the cells contract. The resulting heartbeat in the ECG is manifested by a series of waves whose timing convey and morphology information which are used for diagnosing diseases, indeed they are the mirror of disturbances of the heart's electrical activity. The time pattern characterizes the occurrence of successive heartbeats and its also very important. A group of cells simultaneously depolarizing can be seen as an equivalent current dipole associated with a vector. The vectors describe the time-varying position, orientation and magnitude of the dipole and can be summed to give a dominant vector describing the main direction of the electrical impulse, see Fig. 2.6.

Depending on the location of the electrode the resulting wave can be positive or negative, associated with a vector directed towards or away from the electrode respectively. Referring to an healthy ECG, as shown in Fig. 2.7, it is possible to distinguish the most importanT waves.

P wave

It is associated with atrial depolarization

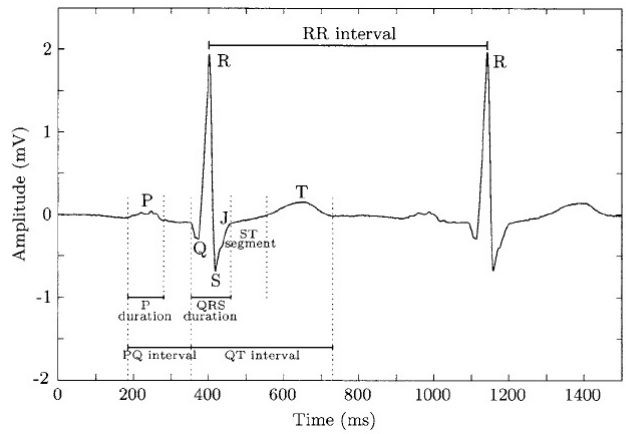

Fig. 2.7: Wave and interval definitions of two consecutive heart-beats [13].

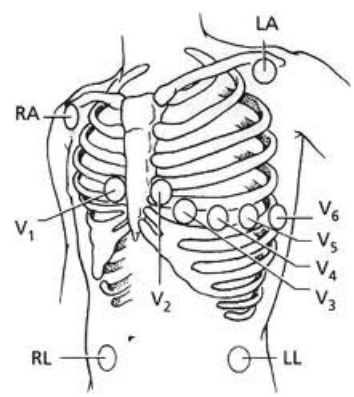

Fig. 2.8: Mason-Likar 12-lead ECG system [14].

QRS complex
: It is composed by three waves which correspond to ventricular depolarization; following the order we have the depolarization of three heart regions: inter-ventricular region (Q wave), left ventricle apex(R wave), basal region and posterior left ventricle(S wave)

T wave
: It represents re-polarization of ventricles.

U wave
: As T wave, it has low amplitude value. It represents the re-polarization of papillary muscles

The diagnosis of cardiac pathologies is based on the abnormal presence of these waves. Besides, not only the single waves are taken account, but also specific time interval between them. This impulse is recorded by a set of leads which have a standard position on the body surface. Up to twelve different leads are used when taking an ECG. Each lead is measured between a pair of electrodes placed at different locations on the chest or body, see Fig. 2.8

2.5 Atrial Fibrillation

Complications	Relative changing in AF patients
Death	Death rate doubled
Stroke	Stroke risk increased
Hospitalizations	Hospitalizations are frequent in AF patients and may contribute to reduced quality of life.
Quality of life and exercise capacity	Wide variation according to AF classification and presence of other pathologies
Left ventricular function	Wide variation according to AF classification and presence of other pathologies

Tab. 2.2: Complications enhanced in the overview of Kirchhof et *al* [15].

Atrial fibrillation is the most common arrhythmia [1]. The rise in the prevalence of AF can be predominantly attributed to ageing of the population and to a higher incidence of cardiovascular diseases. Stroke is the most

debilitating complication of AF, being associated to hypercoagulable state, structural abnormalities in the fibrillating atria, and relative blood stagnation. During AF multiple foci are present in the atria, thus the electrical impulses in the upper chambers of the heart, becoming chaotic and cause an irregular heartbeat. This irregular atrial depolarization causes the P waves to disappear on the ECG, where the baseline becomes fibrillating (f waves). The irregular heartbeat can result in heart palpitations along with a variety of symptoms such as fatigue. When the heart is not pumping blood effectively, blood can stagnate and clot. If the clots break apart and travel to the brain, they can cause a stroke, which represents one of worst consequence linked to AF. In general, the diagnosis is made on the basis of the irregularity of the ventricular rhythm and the absence of P waves on the ECG, see Fig. 2.9. In Tab. 2.2, it reports the most important outcome parameters caused by AF.

Fig. 2.9: Comparison of ECG tracks during normal rhythm (upper image) and AF (lower image) [16].

2.5.1 Diagnosis and Classification

The fast atrial activity, irregular in its shape and chronology, is not always visible in a non-optimal technical quality recording, in which case the diagnosis is essentially made on the irregularity of the ventricular complexes, see Figure 2.10. The presence of AF as the basic rhythm of the recording makes the ECG interpretation much more difficult because the appearance of the next ventricular complex cannot be foreseen [17]. As it has been said above, the electrocardiographic diagnosis of AF is given by the presence of rapid atrial activity which is irregular (more than 400 bpm), with ventricular activity appearing with QRS complexes separated by RR intervals which are completely irregular. AF can be the basic rhythm or it may be present in episodes that can be long or short, alternating with another basic rhythm, usually the sinus rhythm.

Although there is a well-accepted classification, as it shows the next de-

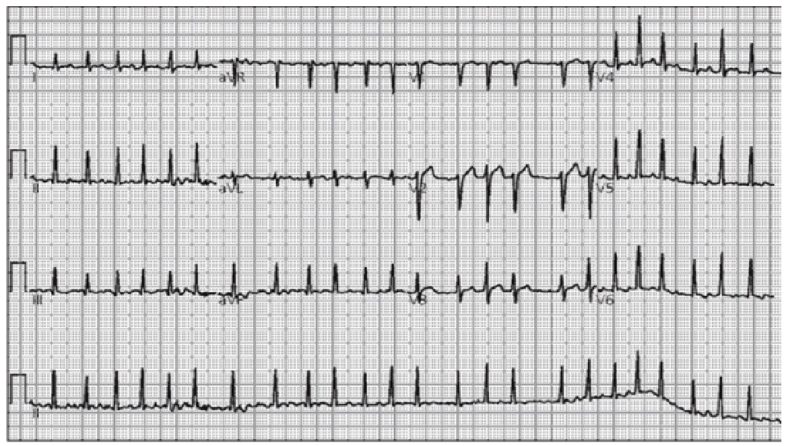

Fig. 2.10: ECG during Atrial Fibrillation [17].

scription according to the guideline interpretation [18], it is not likewise true for the mechanism which bring manifestation of the arrhythmia [19].

Paroxysmal AF

The word paroxysmal means recurring sudden episodes of symptoms. It means that sporadic episodes of AF come and go. The presence of each episode comes on suddenly, but will stop without treatment within a week (more commonly within two days). So each episode stops just as suddenly as it starts and the heartbeat goes back to a normal rate and rhythm. For this reason the interval time between each each paroxysmal episode can vary widely from patient to patient. Although paroxysmal AF means that it will stop on its own, some people with paroxysmal AF take treatment as soon as the AF develops, to stop it as quickly as possible after it starts.

Persistent AF

This means AF that lasts longer than seven days and is unlikely to revert back to normal without treatment. However, the heartbeat can be reverted back to a normal rhythm with cardioversion treatment. Persistent AF tends to be recurrent so it may come back again at some point after successful cardioversion treatment.

Long-standing persistent

AF has lasted for more than one year when it is decided to adopt a rhythm control strategy.

Permanent AF

This means that the AF is present long-term and the heartbeat has not been reverted back to a normal rhythm. This may be because cardioversion treatment was tried and was not successful, or because cardioversion has not been tried. People with permanent AF are treated to bring their heart rate back down to normal, but the rhythm remains irregular. Permanent AF is sometimes called established AF.

2.5.2 Treatment

During AF the AV node receives continuously irregular atrial impulses that create shorter and more irregular RR intervals than during normal sinus rhythm. Thanks to the AV node, the impulses are mostly blocked and they cannot reach the His bundle. Nowadays there are two principal ways to manage the arrhythmia: to restore and to maintain sinus rhythm, or to let AF to continue avoiding rapid ventricular rates. The former is called rhythm control, while the latter is rate control.

Restoration of sinus rhythm

One of the treatment to restore sinus rhythm is the pharmacological cardioversion, i.e., antiarrhythmic drugs to stop the AF episode. The pharmacological cardioversion is more effective on patient with paroxysmal AF, where the remodelling is limited. Taking apart the pharmacological treatments which aim the restoration of sinus rhythm, we expose briefly two different techniques for the goal before-mentioned: DC (Direct current) cardioversion and catheter ablation.
DC cardioversion is applied in those cases where the arrhythmia is classified as persistent [20]. This technique concerns uses a therapeutic dose of electric current to the heart at a specific moment in the cardiac cycle. Two electrode pads are used which are connected by cables to a machine which has the combined functions of an ECG display screen and the electrical function of a defibrillator. Recording the DC cardioversion event with an ECG, it look as shown in Fig. 2.11.
Instead, catheter ablation should be reserved for patients with AF which remains symptomatic despite optimal medical therapy. The ablation consists to an invasive procedure, which includes the use of radio-frequency energy. This energy creates a "scar", which stops the fast, irregular impulses from the atria reaching the ventricles, this will stop your fast heart rate. Long-term follow-up of these patients suggests that while sinus rhythm is better preserved than with antiarrhythmic drugs, late recurrences are not uncommon.

Rate control

The rate control during AF is broadly defined as prevention of inappropriately rapid and irregular ventricular rates during AF without making any specific attempt to restore and maintain sinus rate. Rate control in AF has three aims: control of the heart rate at rest, control of the heart rate during activity, and regularization of the heart rate. Control of the ventricular rate is a crucial goal of pharmacological management of AF. The combination of drugs to be given to a patient is obviously based on the classified AF and presence of other heart diseases.
Usually, it is considered by medical staff a long-term treatment. The main motivation to initiate rate control therapy is relief of AF-related symptoms. Conversely, asymptomatic patients should not generally receive rate-control drugs. According to Vaughan Williams classification [22], [23], it groups them based on the primary mechanism of its antiarrhythmic effect. Giving some example, there is the β-blockers group which belongs mainly to I and II class, as *Sotalol, Carvedilol, and Metoprolol*, others examples are *Propafenone, Flecainide* of IC class (I class, it also subdivided in three categories A, B, and C), and *Dronedarone, Amiodarone* of the III class.
All of them achieve the same goal which prevents very high ventricular rate during AF. Their main difference concerns the efficacy and applicability. AF occurring in patients with little or no underlying cardiovascular disease can be treated with almost any rate-control drug that is licensed for AF therapy. Most patients with AF will receive β-blockers initially for rate control. Amiodarone is reserved for those who have failed treatment with other rate-control drugs or have significant structural heart disease. However, the presence of another heart disease can shift the pharmacological treatment to another therapy.

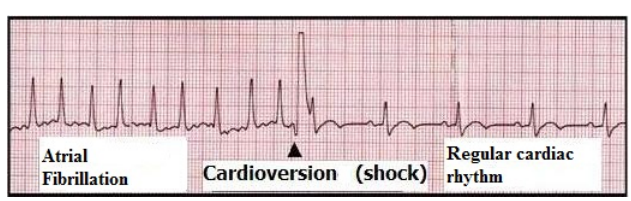

Fig. 2.11: ECG shows the transition from AF-state to the normal rhythm [21].

2.5.3 Investigation technique: RR-Histogram

In the analysis of ventricular response during AF, multimodal histograms have been used as noninvasive support for identification of multiple intranodal pathways in patient with AF. Olsson et al. [24] have made twenty-four-hour ambulatory ECG recordings in patients with mitral valve disease and sustained atrial fibrillation. They segmented the RR intervals series according to defined mean heart rate and constructed different histograms varying the heart rate (called heart-rate stratified histograms). For each heart-rate level varied during normal daily activities from 50-60 to 160-170 *bpm* (obtained by modifications in autonomic nervous tone), they studied the distribution of RR-intervals presented by histograms. Under the condition of wide range of average heart-rate levels the analysis revealed a bi- or trimodal RR-distribution in almost all patients, supporting the hypothesis that atrioventricular conduction occurs via two pathways with separate conduction properties. Restricting the study to bimodal analysis, the two peaks are considered to contribute equally to the distribution of RR intervals. The first peak is made up of RR intervals and represents ventricular excitation induced by slow conduction via AV node. The second peak corresponds to the intervals preceding narrow QRS complexes, representing the fast conduction. It is important to notice the transition from the slower peak towards the faster peak along the decreasing of heart rate, see Fig. 2.12. By their assumption, the heart-rate levels ranging between 90 and 120 bpm are optimal for the demonstration of bimodality. The conclusion to which Olsson arrived, is that, "with highly probability, the changes of the first peak values, induced by variations in autonomic tone, produce changes in the refractoriness of the fastest conducting part of the AV junction". Similarly, it seems likely that the changes of second peak values are referred to changes in the refractoriness of the slower conduction system within AV junction. They also suggest that "AV nodal conduction during atrial fibrillation follows a distinct pattern in human hearts with a presumed normal AV-node". At high heart beats, conduction occurs mainly via fast route, while, at lower ventricular rates, this route is increasingly blocked and conduction occurs via the slower route. see Fig. 2.13.

Thus the concealed conduction model in AF in which the fast and the slow pathaways have different refractoriness, may explain bimodal RR distribution during a random, high rate proximal signal input into a single atrioventricular route.

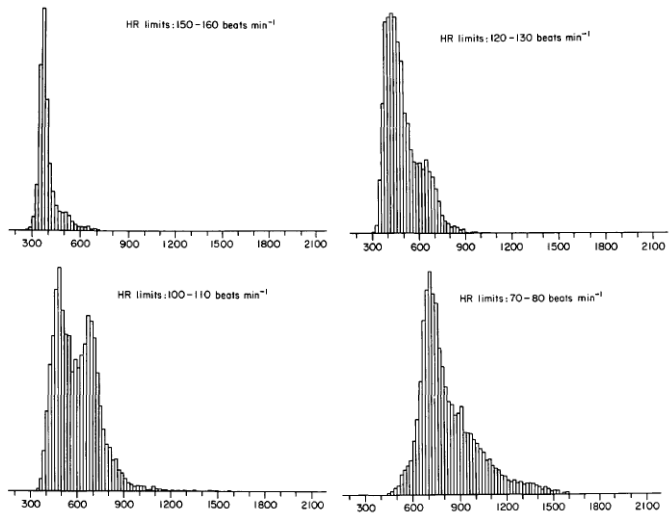

Fig. 2.12: RR normalized histograms.It is possible to notice the bimodal distribution in the histograms between 90 and 130 bpm and possible bimodal distribution in heart rates between 120 and 150 bpm[24].

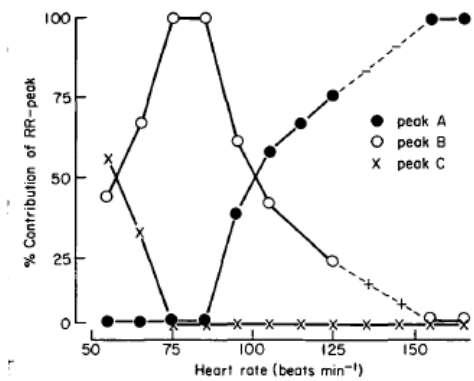

Fig. 2.13: Relative contribution of different peaks of RR intervals at different average heart-rate levels. Note the transition between the peak B (representing the slow pathway) and the peak A (representing the fast pathway)improving the heart rate. The peak C is a possible RR intervals cluster found at lower heart-rate levels and has been defined as a nodal escape rhytm[24].

2.6 Atrioventricular node anatomy

The AV node is located in the so-called "floor" of the right atrium, in the center of Koch's Triangle, over the muscular part of the AV septum, and inferior

to the membranous septum. The AV node has the main role of delaying atrial impulses by approximately 0.12 s. This delta in the cardiac pulse is extremely important. It ensures that the atria have ejected their blood in the ventricles. In the normal heart the cardiac impulse is generated in the SA node and is conducted through the atrial myocardium to the AV node. The compact AV node is a complex histological structure, which consists of a loose transitional zone of cells extending into the surrounding atrial myocardium [25]. These transitional cells are situated in the triangle of Koch, where two pathways arise for the conduction of the impulse: a fast pathway, located anteriorly and in close proximity to the His bundle, and a slow pathway, situated posteriorly and inferiorly to the compact node. The fast pathway conducts more rapidly, usually with a relatively longer refractory period, whereas the slow pathway conducts more slowly, with a shorter refractory period. This section will be characterized by a deeper exposition of AV node characteristics and its conduction properties.

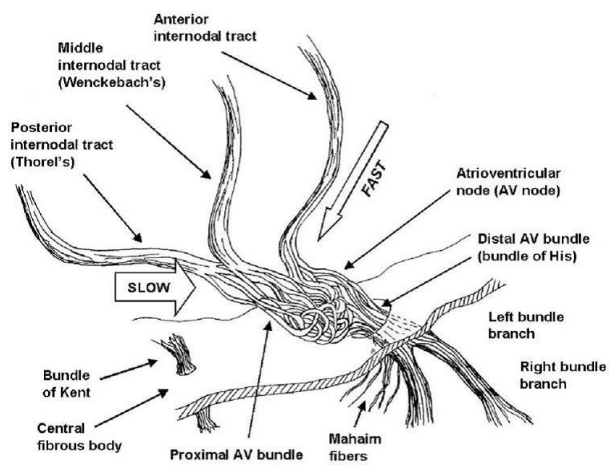

Fig. 2.14: Details of the AV nodal region. The so-called slow and fast conduction pathways are indicated by the arrows (their size was increased to allow the reader to visualize the tortuosity of the conduction pathway) [26].

2.6.1 Dual pathway

As previously mentioned, one of the more intriguing behaviours of the AV conduction is the so-called dual pathway AV node electrophysiology. This term is used in reference to two different T wave fronts that propagate from the atria to the His bundle, one with a shorter effective refractory period

(ERP) and another with a longer ERP (i.e. slow and fast pathways respectively). This phenomenon was described during 1950s by Preston and collaborators [27], nowadays the role that fast and slow wavefronts play in the conduction from the atria to the His bundle remains unclear. In fact, the evaluation of their individual influence on the AV nodal conduction is not possible since the pathway responsible of the each AV conduction could not be identified. The demonstration of the existence of two pathways has been well documented by N. Mazgalev et al. [28] that has performed invasive studies using 10 rabbit during AV node reentrant tachycardias. According to their model, the AV node is a bilayer structure supported by two wavefronts. An earlier wavefront (fast) that propagates via the transitional cell envelope, and a later wavefront (slow) propagates via the deeper inferior nodal extensions. They have studied the AV node potential depending on the distance measured in time between two consecutive atrial impulses (A1A2). The decrease of A1A2 was associated with a decrease in AV node potential with consequent AV node block, suggesting that the available driving force was unable to generate full depolarization. When A1A2 was shortened to threshold value, the presence of a delayed component, representing the later and stronger slow wavefront, let the restoration of the conduction, and a full AP.
The slow and fast pathways are physiologically and anatomically distinct routes to the AV node. The slow pathway traverses the isthmus between the coronary sinus and the tricuspid annulus and has a shorter effective refractory period but a longer conduction time compared to the fast pathway. The collocation of the fast pathway is usually in the interatrial septum, and it is characterized by a faster conduction rate and a longer effective refractory period. During the sinus rhythm the normal conduction happens along the fast pathway, but during pathologies like AF, where it occurs a higher heart rates, possible premature beats are often conducted through the slow pathway, since the fast pathway can be refractory at these rates. More specifically, the dual characteristics of this function have been revealed using an *S1-S2 pacing protocol*; in this procedure, a stimulus (S1) of constant duration and amplitude was given and after followed by a second stimulus (S2) of varying duration and amplitude. At each step, the S1-S2 interval was reduced until conduction block in the fast pathway occurs due to the long refractory period [28]. Thought the primary function of the AV node may seem simple, that is to relay conduction between the atria and ventricles, its structure is very complex.

Merging the two most important topics (AF and dual pathway), during AF the time between two atrial activations is shorter than the refractory period of AV nodal cells. Consequently, the AV node works as a filter, blocking

some atrial activations and limiting the number of ventricular beats. The way in which this natural filter works, and how it could be used to perform efficient rate control therapies, remains not completely understood. Next two paragraphs prove the differences between the two pathways, following several experimental investigations.

Slow Pathway

Supported by mapping and catheter ablation studies, Mcguire et *al.*[29] have shown as depolarization of the AV junctional tissue coincides temporally with the slow component of slow pathway potentials. Since AV junctional cells have nodal-like APs, they have the necessary characteristics for slow conduction. During their experiment they have given adenosine in blood-prefused dog and pig hearts,that provokes in cells with nodal-type APs, a reduction in AP amplitude and duration. So using adenosine, the conduction in both the slow pathway and the AV junctional cells has been registered. The AV junctional cells in the posterior nodal approaches are in electric continuity with the atria and AV node but can be electrically dissociated from the atria and the AV node fast pathway through pacing techniques[29]. Moreover, these AV junctional cells are depolarized before the earliest atrial activation during retrogade slow pathway conduction but are not depolarized during anterograde fast pathway conduction, it means that these cells could be the substrate of the slow pathway. However this hypothesis is not completely confirmed by the author Mcguire et *al.*

Fast Pathway

The placement of fast pathway has been suggested at the anterosuperior perinodal tissue, proximal to the His bundle [30]. It has been shown in patients with AV nodal reentry tachycardia, that radiofrequency catheter ablation anteriorly produces precise electrophysiological effects. Although few patients still have dual AV nodal physiology, most have a continuous curve similar to the slow pathway portion of the AV nodal function curve before ablation, see Fig.2.15. These observations suggest that applying anterior lesions produces a selective effect on fast AV nodal pathway function in patients with typical AV nodal reentry tachycardia.

Concealed Conduction

It has well documented that an impulse entering the AV node can sometimes fail to traverse it completely. Langerdorf[31] used for the first time the term "concealed conduction" to describe this phenomenon, whose behaviour is

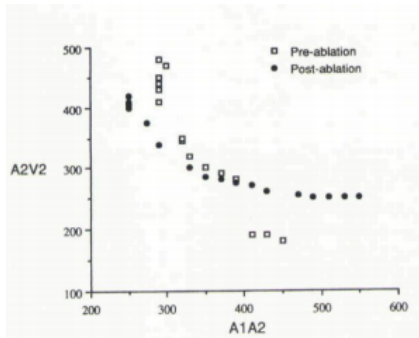

Fig. 2.15: Atrioventricular nodal function curves before and after anterior ablation. The AV nodal function curve before ablation is represented by the open squares and after ablation by the solid circles. It is possible to note the disappearance of the fast pathway portion of the curve after ablation [30].

described as "the presence of incomplete conduction coupled with an unexpected behaviour of the subsequent impulse".
At the beginning the use of this term was restricted to define:"(1) partial or incomplete forms of anterograde and/or retrograde AV conduction block in which an atrial impulse did not generate a distal response but had influences on impulses that followed it; (2)"abortive AV node conduction of a premature atrial impulse blocked in both directions causing first or second degree AV block". Over the years, it was discovered that the blocked impulses brought to a general increase refractoriness of the same AV node, whose conduction time is delayed by these following characteristics: strength,direction, form, number and sequence of the fibrillatory impulses that reach the AV node. Accordingly, this activity is underlined by slow irregular ventricular rhythm during AF. In the following paragraph it is explained what mechanisms have been introduced to understand this phenomenon.

Electrotonic modulation and decremental conduction

The mechanism controlling the concealed conduction is still controversial. According to Hoffamn's[32] previous work, the AV node is "the site for slow and continuous conduction of electrical impulses from the atrium to the His bundle". The effects that may be develpoed by the crossing of the impulses across the AV node are a progressively increasing threshold, a decreasing amplitude and because of the raising rate of the AP there would be a gradual decrease of activity of the regions responsible for depolarizing more distal tissues.

However Meijler et *al.* confuted the decremental conduction existence bringing different considerations. At first it is quite clear that the AV conducting system should be regarded as highly heterogeneous and discontinuous. Moreover, it is incompatible with the modern electropydiological properties and with the electrocardiographic features recorded in patients with AF. So a new idea was proposed, linked to the existence of electrotonic modulation of AV node propagation by atrial impulses blocked within the AV node, responsible in the irregular rhythms noticed in patients with AF. While in decremental conduction the amplitude of the AP decreases gradually until it dissipates completely, unable to excite tissues ahead of it, in electrotonic transmission, the AP stops at the site of block. Thanks to the local circuit, there will be a passive membrane depolarization whose amplitude decays with the distance, as function of the resistive properties of the tissues involved.
Meijler has explained the presence of "after effects" on the propagation of subsequent impulses, when the concealed conduction happens. When an impulse is blocked in the AV node, a subthreshold depolarization for cells distal to the site of block verifies. Therefore the inibition of amplitude brought by the subthreshold depolarization will affect the second AV node subthreshold response(defined as electrotonic effects). The whole effect produces a delay or even a blockade in the transmission of the subsequent impulses.

Chapter 3

Mathematical Background

In this chapter there is an overview of the mathematical knowledge necessary for the implementation of the AV node model.

3.1 Poisson Process

The Poisson process is defined as a stochastic process that counts the number of arrivals $N(t)$ occurred in the finite interval time of length t with a mean rate λ defined as intensity, see Fig. 3.1. The function $N(t)$ obeys to the Poisson

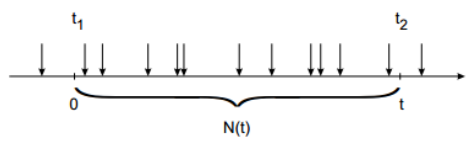

Fig. 3.1: Given the interval time t, N(t) represents the number of randomly in time arrivals

distribution:

$$P\{N(t) = n\} = \frac{(\lambda t)^n}{n!} \exp\{-\lambda t\} \tag{3.1}$$

where λt is the mean of events that will occur during the time t. If the intensity λ is constant, the process is called homogeneous, otherwise if $\lambda(t)$ is time-dependent, the process is an inhomogeneous Poisson process, and the average arrival rate in the interval time [0;t] of the Poisson process will be:

$$\mu(t) = \int_0^t \lambda(\tau)\, d\tau, \;\; t \in \tau \tag{3.2}$$

The Poisson process has some peculiar properties that will be described below.

Memoryless property: An X process can be characterized by *memoryless property* if:

$$Pr\{X > t + x\} = Pr\{X > x\} \tag{3.3}$$

Considering X as the waiting time until some given arrival, the equation 3.3 states that, given that the arrival has not occurred by time t, the distribution of the remaining waiting time is the same as the original waiting time distribution, so the remaining waiting time has no 'memory' of previous waiting. This property implies that the arrivals are distributed randomly in time that assures them the statistically independence.
Assuming this property, it is possible to study the distribution of the interarrival times that occurs along a decreasing exponential controlled by λ:

$$Pr\{interarrival > t\} = \exp\{-\lambda t\} \tag{3.4}$$

Random selection: If a random selection is made from a Poisson process with intensity λ such that each arrival is selected with probability p, independentely of the others, the resulting process is a Poisson process with intensity $p\lambda$.

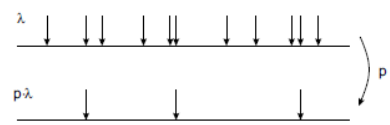

Random split: If a Poisson process with intensity is randomly split into two subprocesses with probabilities p_1 and p_2, where $p_1 + p_2 = 1$, then the resulting processes are independent Poisson processes with intensities $p_1\lambda$ and $p_2\lambda$.

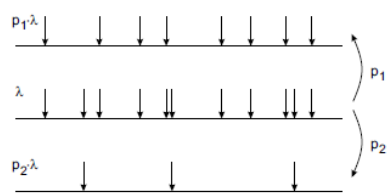

3.2 Maximum Likelihood Estimation

The method of maximum likelihood (MLE) [33] corresponds to many well-known estimation methods in statistics. MLE is a preferred method of parameter estimation in statistics and is an useful tool for many statistical modeling techniques.
Let define $y = (y_1, ..., y_m)$ that corresponds to a random sample vector from an unknown population. The aim of this algorithm is represented by the set of parameters that generate the most likely sample. Here, each population has correspondent probability distribution and with each probability distribution an unique parameter. Defined $p(y|\theta)$ as the probability density function (PDF), it specifies the probability of observing data vector y given the parameter θ. The parameter $\theta = (\theta_1, \ldots, \theta_k)$ is a vector in a multi-dimensional

parameter space. Assuming all elements y_i of $\mathbf{y}$ are statistically independent, second to theory of probability, the PDF for the data $\mathbf{y} = (y_1, ..., y_m)$ given the parameter vector θ can be expressed as a production of PDFs for individual observations:

$$p(\mathbf{y} = (y_1, y_2, \ldots, y_n)|\theta) = p(y_1|\theta) * p(y_2|\theta) * \ldots * p(y_m|\theta) = \prod_{i=1}^{m} p_i(y_i|\theta) \tag{3.5}$$

Denoting the inverse problem: *Given the observed data and a model of interest (set of parameters), find the one PDF, among all the probability densities that the model describes, that is most likely to have produced the data.* It is useful work with the natural logarithm of the likelihood function, the so-called $log-likelihood$ function:

$$logp(y|\theta) = \sum_{i=1}^{m} logp_i(y_i|\theta) \tag{3.6}$$

The final solution is given by the maximization of Eq. 3.5, obtaining formally,

$$\hat{\theta} = argmax_\theta \Big\{ p(y|\theta) \Big\} \tag{3.7}$$

The value $\hat{\theta}$ is called the maximum likelihood estimate of θ. The solution to the equation may not have a close form solution because of the complexity of the model (high parameter number), therefore it becomes necessary to solve the problem numerically (see next section). Below, MLE properties are listed:

Consistency. The sequence of MLEs converges in probability to the value being estimated [34].

Asymptotic normality. As the sample size increases, the distribution of the MLE tends to the Gaussian distribution with mean θ and covariance matrix equal to the inverse of the Fisher information matrix [34].

Efficiency. It achieves the Cramér−Rao lower bound when the sample size tends to infinity. This means that no consistent estimator has lower asymptotic mean squared error than the MLE (or other estimators attaining this bound)[35]. Second-order efficiency after correction for bias [36].

3.3 Optimization Algorithms

In general, an optimization problem can be express as:

$$z = argmax\Big\{ f(x) \Big\} \tag{3.8}$$
$$x \in X$$

where:

- X array of admissible solutions
- $f(x)$ target function to maximize (or minimize)

Discerning the difference between local and global maximum, we say that a specific $x^* \in X$, we will have:

- $f(x^*) \geq f(x), \forall x \in \mid \varepsilon(x)$, where $\varepsilon(x)$ is part of X (Local)
- $f(x^*) \geq f(x)\ \forall x \in X$ (Global)

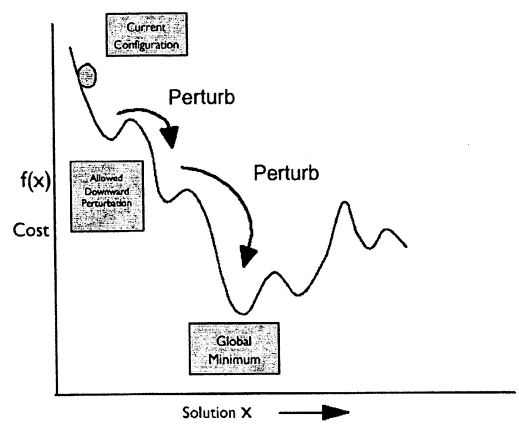

Fig. 3.2: Example 2-D of a general optimization problem [37].

For non-determistic polynomial-time hard (NP-hard), computationally burdensome, usually it is necessary to apply heuristic methods for reaching the solution. We can divide the procedure in two iterative techniques: building and improving. The first is geared to find an admissible solution; while the second, starting from the admissible solution previously found, iteratively applies a function, converging to the local maximum. The main problem, given by heuristic algorithm, is the "local solution trap", which can be bypass using

proper converging procedure that it allows to accept worse solutions. During the thesis work, we have mainly used the two following algorithms, focusing on them because they represent the best solution (according to the estimation) we obtained. As the most part of iterative algorithms of minimization (or maximization), numerically algorithms suffer about: presence of local minima, long computational time (if the observation number is considerable high). It is also truth that given a certain number of parameters to estimate, the computational increase proportionally to number of parameters. In Fig. 3.2, a bidimensional example shows the research of the optimal solution (global minimum).

3.3.1 Simulated Annealing

As above mentioned, there are two techniques to find the solution. The success possibility increase often using metaheuristics techniques, as simulated annealing (SA) [38]. It is based on the analogy between the hardening physic process and the solving of combinatorial optimization problems. Hardening involving heating and controlled cooling of a material to increase the size of its crystals and reduce their defects. Both are attributes of the material that depend on its thermodynamic free energy. Heating and cooling the material affects both the temperature and the thermodynamic free energy which are differently correlated. While the same amount of cooling leads the same amount of decrease in temperature it will lead a bigger or smaller decrease in the thermodynamic free energy based on the rate that it occurs, with a slower rate producing a bigger decrease. The notion of slow cooling is implemented in the SA algorithm as a slow decrease in the probability of acceptance worse solutions as it explores the solution space. Indeed, accepting worse solutions is property of metaheuristics because it allows for a wider search for the optimal solution. Describing in summary the macro-steps, we would have:

Initialization:
Starting initial guess point (S).

Move definition:
Define the operation to find a random S' solution around the current solution.

Accepting the move:
Assessing or not S' solution as new current solution, so $S' \rightarrow S$, apply-

ing the following accepting probability:

$$P = \begin{cases} 1 & \Delta_f \leq 0 \\ e^{(-\frac{\Delta_f}{T})} & \Delta_f \geq 0 \end{cases}$$

Cooling schedules:

It represents all control parameters of SA. In general, it is composed by: initial control parameter (T_0), allowing at the starting point to all transition to be accepted; final control parameter (T_f), no transition is accepted; transition number L_k for each value T_k and decremental law T; they are correlated to ensure a quasi-equilibrium condition for each T value changing.

Our choice fell on the use of pattern search, being more time-efficient.

3.3.2 Generalized Pattern Search

The patternsearch is a *direct search method* for solving non linear optimization problems [39], it means that it does not use derivatives or approximations of derivatives to solve the problem:

$$min_x f(x),$$

where $x \in R^n f : R^n \to R$. A subset of the direct search algorithms, class called *pattern search*, share a structure that makes unified convergence analysis. The general form of optimization is given by an initial guess at a solution x_0 and an initial choice of a step length parameter $\Delta_0 > 0$. The algorithm can be explained as following:

For $k = 0, 1, ...,$
i) Check for convergence;
ii) Compute $f(x_k)$;
iii) Determine a step s_k using *exploratory moves* (Δ_k, P_k);
iv) If $f(x_k) > f(x_k + s_k)$, then $x_{k+1} = x_k + s_k$, otherwise $x_{k+1} = x_k$;
v) Update (Δ_k, P_k).

The *pattern* P_k is defined by two components, a real nonsingular *basis matrix* B and a *generating matrix* C_k, where the columns of C_k must contain a *core pattern* represented by M_k and its negative $-M_k$. The pattern P_k is then defined by the columns of the matrix $P_k = BC_k$, therefore the steps are of the form $s_k = \Delta_k B c_k$, where $c_k \in C_k$.

The hypothesis required by the *exploratory moves* are:

i) $s_k \in \Delta_k P_k \equiv \Delta_k BC_k$;
ii) If $min\{f(x_k+y), y \in \Delta_k B[M_k, -M_k]\} < f(x_k), then f(x_k+s_k) < f(x_k)$.

The second hypothesis claims that if descent can be found for any one of the $2n$ steps defined by the core pattern, the *exploratory moves* returns a step that gives a simple decrease and the iteration is considered *successful*. If the iteration is *unsuccessful* it is required to reduce the current step-length control parameter Δ_k,which has the effect of refining the restriction, called rational lattice, over which the search is conducted. The process will be repeated until some suitable stopping criterion is satisfied.
The advantages of the algorithm are given by the mild conditions on both the *exploratory moves* and the Δ_k update to guarantee global convergence. There is no requirement that the step should be defined by the core pattern, nor that $2n$ steps must be evaluated, or even that the step returned gives the greatest decrease possible.

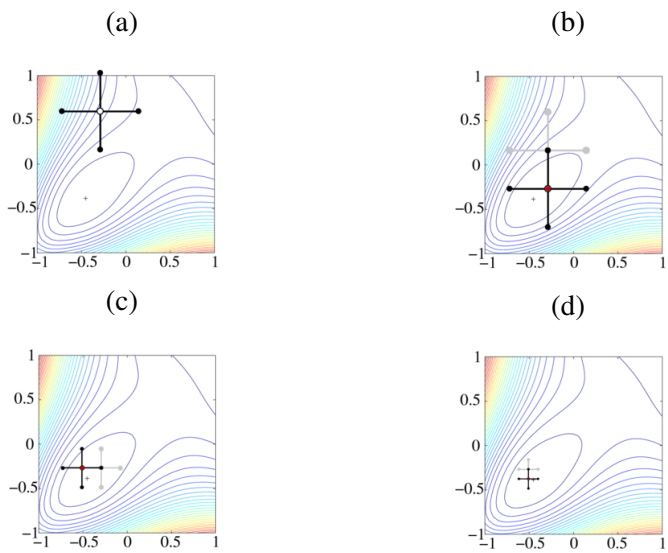

Fig. 3.3: The figures (a), (b), (c), (d) represent an example of convergence of pattern search finding the global minimum, where warm colors are high values and vice versa [40].

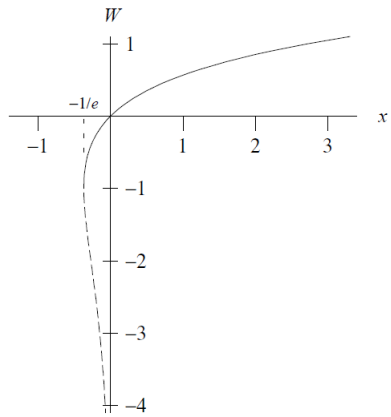

Fig. 3.4: The two real branches of $W(x)$. The first dashed line is $W_0(x)$;the second continuous line is $W_{-1}(x)$[41]

.

3.4 Lambert Function

The Lambert Function is defined to be the multivalued inverse of the function[41]:

$$x = W(x)e^{W(x)} \tag{3.9}$$

In case of real x, for $\frac{1}{e} \leq x < 0$ there are two possible real values of $W(x)$, see Fig. 1.2. The branch satisfying $-1 \leq W(x)$ is called the *principal branch* ($W_0(x)$) and the branch satisfying $W(x) \leq -1$ the *negative branch* denoted as $W_{-1}(x)$. The negative branch goes to $-\infty$ as $x \to 0$, while the principal branch grows slowly but unboundedly for $x \to \infty$

The behaviour of the Lambert W function can be understood by comparing it to the natural logarithm, the inverse of e^w, where w is assumed equal to $W(x)$. For large negative or positive $w =$, e^w and we^w grow similarly, so their respective functions have similar asymptotes. Multiplying the exponential for w deforms its graph around 0 so that it is no longer monotone, and that is why the Lambert W has two real branches: one for values on each side of the stationary point, see Fig. 3.5. The Lambert W function solves any equation of the form $C = xe^x$, defined as *canonical form*. So, given the equation $xb^x = a$, the solution is:

$$x = \frac{W(a\log b)}{\log b} \tag{3.10}$$

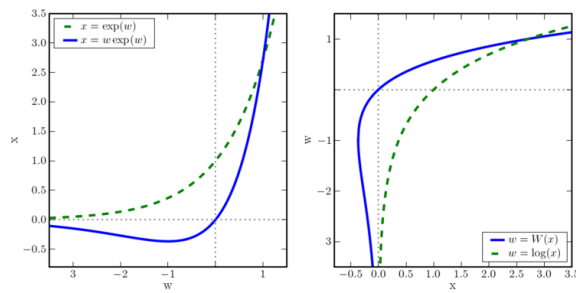

Fig. 3.5: The following plots represent the relation between the two exponential functions (left graph) and their inverse function (right graph)[42].

Chapter 4

Methods

The following chapter provides in the first part an overview of previously proposed previous mathematical models of the AV node conduction system. The non invasive model proposed by Corino *al.*[4] is thoroughly described since this thesis is based on it. The last paragraph accounts the principal modifications that have been implemented to the previous model.

4.1 Previous mathematical AV node models

Several mathematical models have been proposed to study the AV nodal electrophysiological characteristics. The models can be estimation models, (cf. Mangin model in Sec 4.1.1), or simulation models, (cf. Cohen model in Sec 4.1.2 and Lian model in Sec 4.1.3). The clinical information used by the models could be divided in invasive or non-invasive. The invasive information can be useful for the simulation models to have a comparison of the results, while the estimation models apply this information to obtain the estimated parameters. Estimation models are based on the mathematical model taking into account the most important electrical properties of AV node described by model parameters. The main problem related to this approach is the simplification needed to describe the AV node. The other way proposed is creating a simulation of the AV node that is able to describe a more detailed characterization of electrophysiological dynamics. However it cannot ensure a unique estimation of parameters; it means that they are not suited for a robust estimation. In the following paragraphs several models are considered for each most commonly technique used to acquire information from AV node conduction system.

4.1.1 Mangin model

Mangin et *al.*[43] have studied the effect of metoprolol and amiodarone drugs on atrial and ventricular activity during AF by epicardial recordings in 10 post-surgical patients. The aim of the work was proposing a mathematical

model of AV node, extracting parameters that are able to describe the drug effects on AV nodal physiology during AF. The study is based on the relationship between the AV nodal conduction time and the preceding recovery interval. According to the model, the conduction time is associated with a sequence of conducted beats through an iterative series. The model accounts for the concealed conduction (see section 2.6.1), improving their previous hypothesis that each blocked beat leds to a fixed increment in the refractory period[43]. Mangin et *al.* modified this assumption, supported by recorded data. Since atrial activations show different degrees of penetration of the AV node, due to their time-variability and conduction pathway chosen, it is reasonable, according to them, to estimate the prolongation of the refractory period brought by blocked beats using a normal distribution.
The conclusion to which they arrived was that the drugs effects have led a decrease in ventricular activity, but no marked changes in the atrial activity. So changes in ventricular rate are conducted by alterations in the properties of the AV node, rather than changes in the atrial activity. The main limitation of this model is linked to its nature. Since it is an approximation of the physiological AV node, it is not easy to estimate the errors relative to the parameters. So the relationship between variations in conduction through the AV node and the parameters is still unknown. Moreover, their intention to predict the time of occurrence of every ventricular contraction, it is not possible because of the stochastic nature of the penetration of atrial activity into AV node during AF.

4.1.2 Cohen model

The non-invasive model proposed by Cohen et *al.*[2] has been created for the genesis of RR interval fluctuations during AF and accounts for the statistical features of the RR interval sequence. The modelling AV node is considered as an electrically active cell with defined electrical properties, like refractory period and automaticity. During AF there is a turbulent electrical activity in the atria that leads to arrival atrial impulses randomly in time with greater frequency (called λ) compared to the sinus rhythm frequency. The mathematical assumptions concern the arrival of atrial impulses studied as a Poisson process, and the temporal and spatial summation of the electrical activity of all cells of the AV node. It means that all blocked atrial impulses are summed in time and the AV node do not initiate a new refractory period until after the next ventricular activation has occurred.
Cohen has studied the statistical properties of RR interval, discovering the statistical independence of each other during AF. Indeed, focusing the attention on autocovariance coefficients of RR intervals values, during normal

sinus rhythm the correlation of RR intervals is over delays of 25 ms, while during AF the autocovariance is similar to zero for index $i \geq 2$, see Fig. 4.1. Under this condition it is confirmed the hypothesis of Poisson process for which the process needs to be memoryless (section 3.1).

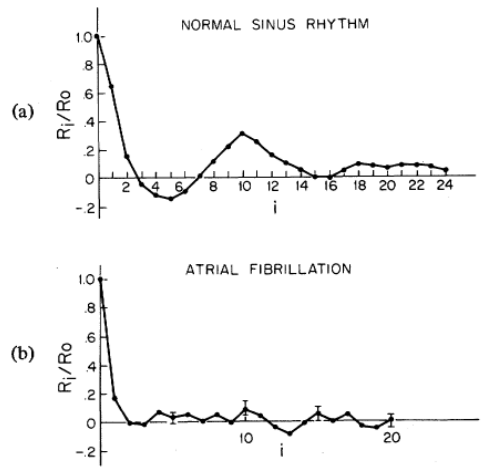

Fig. 4.1: Plot of autocovariance coefficients of RR interval sequences during normal sinus rhythm (a) and during AF (b)[2]

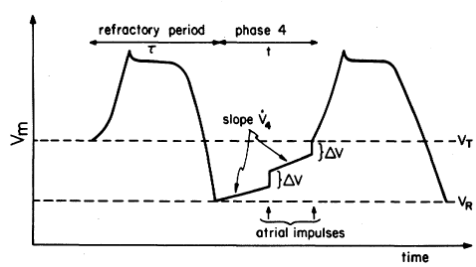

Fig. 4.2: Transmembrane potential of hypothetical AV junction cell. The action potential of duration τ, marks the period during which the AV node is refractory. During the phase 4 the AV node depolarize spontaneously by constant $\dot{V}_4$, and each arrival atrial impulse creates a step-wise depolarization that adds an amount equal to ΔV. When it is reached the threshold V_T a new action potential is ready[2].

In the Fig. 4.2 the transmembrane potential of the AV node is shown. According to this model, there is a time τ during which the AV node is completely refractory by stimulation of atrial impulses. At the beginning of the

phase 4 the transmembrane potential is at its resting potential value V_R. During this phase there are two different ways of transmembrane potential increase: (1) spontaneously rise with a rate equal to $\dot{V}_4$; (2) discrete increase ΔV due to atrial impulse arrival during this period. The threshold V_T could be reached by the result of stepwise depolarizations due to atrial impulses, and spontaneous phase 4 depolarization. After this value the AV node starts to fire by creating a new action potential.
In Cohen's model the amplitude ΔV has two different meanings: (1) it reflects the sustained stepwise depolarization made by the single cells; (2) it represents also the spatial coherence of this activity. Therefore during normal sinus rhythm, a synchronous depolarization wavefront arrives at the AV node with $\Delta V = V_T - V_R$, permitting one-to-one atrioventricular conduction. During AF, there will be the loss of spatial coherence in atrial depolarization that will cause a decreasing in ΔV amplitude. As the degree of spatial disorganization increases, λ raises with the widespread of many parallel inputs to AV node.
The first mathematical model proposed by Cohen takes into account the four parameters:

1 λ is the frequency of atrial impulses that arrive at the AV node;

2 $\Delta V/(V_T - V_R)$ is the relative amplitude of the atrial impulses during phase 4;

3 $\dot{V}_4/(V_T - V_R)$ is the relative rate of phase 4 depolarization of the AV node;

4 τ is the refractory period of the AV node.

One property not underlined by the Fig. 4.2 is the time required by impulses to pass through the AV node. However, according to Cohen's model,since there is the hypothesis of random arrival in time of atrial impulses to the AV node,the RR interval distribution during AF is not influenced by a randomly conduction delay of atrial impulses. Therefore it is not necessary to consider the conduction delay in analyzing the predicted RR intervals histogram.
To have a confirmation of their model, Cohen compared the experimental histogram of RR intervals obtained from patients in chronic atrial fibrillation to the prediction model. The result was that the model was able to predict both unimodal RR intervals histograms, and multiple peaks in the histogram. However two of the four parameters described, $\Delta V/(V_T - V_R)$ and $\dot{V}_4/(V_T - V_R)$, can be uniquely determined only if the histogram is bimodal, since they are useful to define the positions of the two peaks. Moreover, the model

estimates unphysiological values of the parameter λ, range between 5 Hz and 116 Hz. The solution proposed is that λ can not represent the atrial impulses mean rate of a single site, but the summation of impulses derived from many cells.
In this context a more recent work has been made by Corino et *al.*[4].

4.1.3 Lian model

Lian et *al.*[3] have proposed an AF-ventricular pacing model. It could be considered as an extension of Cohen's AF model accounting more detailed electrophysiological characteristics like ventricular pacing, bidirectional physiological conduction delays, and electrotonic modulation in the AV node. In this model both the conduction delay and the refractory period are considered recovery time-dependent; it means that they are connected to the interval between the end of AV node refractory period and the AV activation wave (this interval time is defined in Cohen's model as phase 4).
The concealed conduction related to the atrial impulses is influenced by the electrotonic modulation, as it has been described in section 2.6.1. Each atrial impulse blocked by the AV node, generates a prolungation of refractory period, whose degree is modulated by the electronic modulation and depends from two variables: timing and the strength of blocked impulse. Considering this phenomenon, the ventricular rate could depend from two opposite events:

1 Atrial frequency rate whose increasing frequency provokes a more rapid ventricular rate;

2 the concealed atrial impulses frequency can prolong the AV node refractory period and potentiate the AV block.

So the ventricular rate could depend from the electrotonic modulation level. If it is stronger, the ventricular rate could be slower than atrial frequency impulses, otherwise there will be the opposite event. The strength of this model is that it is taking account for most statistical properties of RR intervals during AF. The weakness is the difficulty to use a simultaneous search over all the sixteen model parameters. They suggest to reduce the dimension of the search space by deriving some baseline parameters indipendently, and thereafter trying to conduct a search, with the reduced space, to achieve quantitative data[3].

4.2 Corino model

The section focuses on the development of the previous work made by Corino *et al.*[4]. The model introduced in this thesis tries to model the AV node dur-

ing AF through ECG-based estimation method [4], taking into account the main electrophysiological properties of the conduction system as its refractory period and related prolongation time, the presence of dual AV pathways.

4.2.1 Description of the model

According to the model, series of AI arrive randomly in time at the AV node following a Poisson process with mean rate equal to λ. The AV node is supposed to be a lumped structure which takes into account the concealed conduction, relative refractoriness and existence of dual pathways.
It is characterized by deterministic time τ, completely refractory to stimulation by AI, and by a stochastic part τ_p, where the transmembrane potential increases uniformly to allow the impulse passing. Thus during the interval time $[\tau, \tau + \tau_p]$, caused by concealed conduction and/or relative refractoriness, the probability to pass is linearly dependent. After the time $\tau + \tau_p$ called maximally prolonged refractory period, no impulse is blocked, see Fig. 4.3.
As described in the section 2.6.1 for each AI there are two ways to reach the

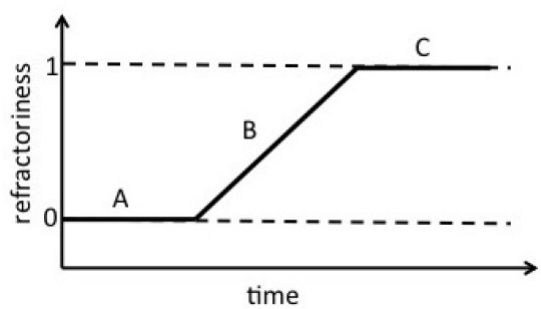

Fig. 4.3: The A tract describes the total refractoriness to the atrial impulses, whereas the B tract indicates a linearly increase of probability of passing from the impulse,in the last C tract all the atrial impulses will pass[44].

AV node: the slow and the fast pathway defined in this model by different refractoriness properties, τ_1 and τ_{p1} for the former and τ_2, τ_{p1} for the latter. The slow pathway, as previously expressed, is characterized by a shorter refractory period, therefore τ_1 is assumed less than τ_2.
The function:

$$p(i) = \begin{cases} \alpha & i = 1 \\ 1 - \alpha & i = 2 \end{cases} \tag{4.1}$$

describes the probability of conduction $p(1)$ through the slow pathway called

α, and hence the probability of conduction $p(2)$ through the fast pathway $(1-\alpha)$. It is possible to define mathematically the refractoriness of the *i*th pathway (i = 1; 2) by the positive-valued function $\beta_i(t)$:

$$\beta_i(t) = \begin{cases} 0 & \text{if } 0 < t < \tau_i \\ \dfrac{t-\tau_i}{\tau_{pi}} & \text{if } \tau_i \leq t < \tau_i + \tau_{pi} \\ 1 & \text{if } t \geq \tau_i + \tau_{pi} \end{cases} \tag{4.2}$$

where t represents the time elapsed from the last ventricular activation, τ_i is the *i*th refractory period and τ_{pi} is the *i*th prolongation time. During the maximally prolonged period, the probability to pass by impulse increases by linearly way. The distribution of non-blocked atrial impulses happens along an inhomogeneous Poisson process with the intensity function $\lambda\beta(t)$. Since the conduction time is included in the function $\beta_i(t)$, the ventricular activation coincides with non-blocked atrial impulse, so also ventricular activations occur as inhomogeneous Poisson process with the same intensity function.
The probability density function (PDF) of the arrival time of the *n*th non-blocked impulse, defined by t_n has the following equation[4]:

$$p_t(t_n) = \frac{\lambda\beta(t)}{(n-1)!}\left(\int_0^t \lambda\beta(\tau)\mathrm{d}t\right)^{n-1} \exp\left\{-\int_0^t \lambda\beta(\tau)\mathrm{d}t\right\} \tag{4.3}$$

Under the hypothesis of temporal coincidence between the arrival atrial impulse and the ventricular activation, the PDF between consecutive ventricular activations, denoted as x, is:

$$p_t(t_1) = p_x(x) = \lambda\beta(x)\left\{-\int_0^t \lambda\beta(\tau)\mathrm{d}\tau\right\} \tag{4.4}$$

Because of the existence of dual pathways, $p_x(x)$ is composed by two components:

$$p_x(x) = \alpha p_{x,1}(x) + (1-\alpha)p_{x,2} \tag{4.5}$$

Combining the time-dependent refractoriness function $\beta(t)$ with the equation 4.4:

$$p_{x,i}(x) = \begin{cases} 0 & \text{if } 0 < x < \tau_i \\ \dfrac{\lambda(x-\tau_i)}{\tau_p} \exp\left\{ \dfrac{-\lambda(x-\tau_i)^2}{2\tau_p} \right\} & \text{if} \tau_i \leq x < \tau_i + \tau_p \\ \lambda \exp\left\{ \dfrac{-\lambda\tau_p}{2} - \lambda(x-\tau_i-\tau_p) \right\} & \text{if } x \geq \tau_i + \tau_p \end{cases} \quad (4.6)$$

where x represents the RR interval. Using the property of statistical independence between consecutive ventricular activations declared in section 4.1.2, the *joint probability function* is given by:

$$p_x(x_1, x_2, ..., x_M) = \prod_{m=1}^{M} p_x(x_m) = \prod_{m=1}^{M} (\alpha p_{x,1}(x_m) + (1-\alpha) p_{x,2}(x_m)) \quad (4.7)$$

where $p_{x,1}(x_m)$ and $p_{x,2}(x_m)$ are obtained by the equation 4.7.

4.2.2 Simulation and Estimation

Input parameters

The set of parameters used for the simulation can be summarized as following:

1 λ is the frequency of atrial impulses. The applied values that can assume are $5.5 \pm 1.5Hz$;

2 $\tau_1 = 0.2 \pm 0.03s$ and $\tau_2 = 0.3 \pm 0.1$;

3 $\tau_{p1} = 0.08 \pm 0.1s$ and $\tau_{p2} = 0.11 \pm 0.04s$;

4 $\alpha \in [0-1]$;

5 nAI is the number of atrial impulses that are assumed to be generated by SA node during the registration time $t = \dfrac{nAI}{\lambda}$. The variation is from 7000 to 15000 impulses.

All the input parameters are estimated from the RR intervals using the maximum likelihood estimation, except for λ parameter. It is determined by the dominant AF frequency λ_{AF} obtained from atrial activity extracted during ECG recordings using spatiotemporal QRST cancellation. However it is necessary to consider atria depolarization time, that accounts a minimum interval

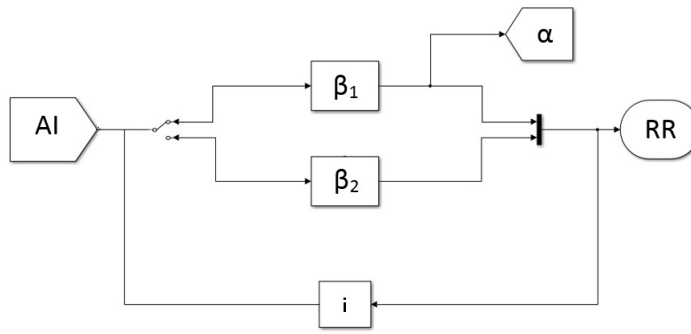

Fig. 4.4: Model of the AV node showing the generator of atrial impulses arriving to the splitter node dividing the two pathways.

time necessary between two successive atrial impulses. Therefore the parameter λ requires to be properly corrected as following:

$$\lambda = \frac{\lambda_{AF}}{1 - \delta\lambda_{AF}} \tag{4.8}$$

where δ accounts the minimum interval time equal to $50ms$.

Simulation

The simulation of RR series has been created by establishing different set of input parameters (previously described), in order to study the shape variations of the RR intervals histogram. In Fig. 4.4 it is shown the general understanding of the model. Referring to the Fig. 4.4, the next atrial impulse arriving after a ventricular activation passes through the slow pathway with probability α. The following atrial impulses follow the pathway chosen by the first one, until one of them is passed. The presence of the feedback let to reset the previous choice related to the pathway taken.
The building of simulated RR interval histogram lets to know the information on the relative frequency of occurence of RR intervals of different lenghts given a fixed set of parameters, see Fig. 4.5.

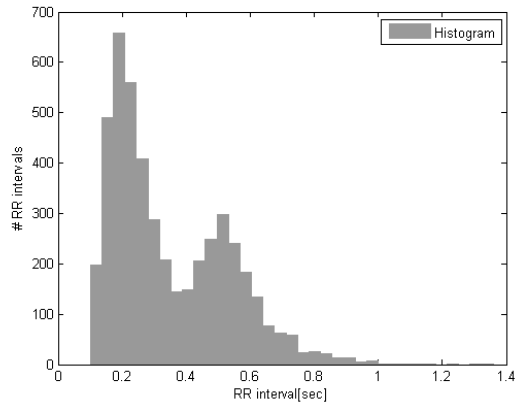

Fig. 4.5: Simulated RR interval histogram during atrial fibrillation. Set parameters: λ=9.09 Hz, τ_1=0.1, τ_2=0.4, τ_{p1}=0.1, τ_{p2}=0.15,α=0.7. Simulated time registration: 27 minutes.

Moreover, the assumption to which the ventricular activations are distributed according to the PDF was verified, by observing the graphical matching between the simulated RR intervals histogram and the PDF given the same set of parameters, see Fig. 4.6. As expected, the two graphs are well overlapped.

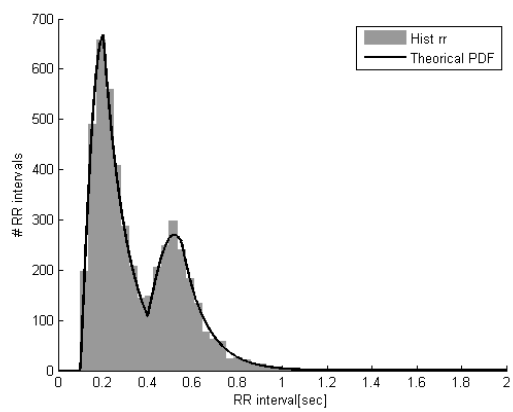

Fig. 4.6: Comparison between RR series histogram and theoretical PDF built through the parameters set: λ=9.09 Hz, τ_1=0.1, τ_2=0.4, τ_{p1}=0.1, τ_{p2}=0.15, α=0.7

Estimation

The estimation of the model parameters related to dual AV nodal pathways and refractory period prolongation contained in the vector

$$\theta = [\tau_1 \ \tau_2 \ \alpha \ \tau_{p1} \ \tau_{p2}] \tag{4.9}$$

have been estimated by jointly maximizing the log-likelihood function respect to θ as following:

$$\hat{\theta} = arg\,max_\theta \, log\, p_x(x_1, x_2, ..., x_M|\theta;\lambda), \tag{4.10}$$

with

$$\begin{aligned} & log\, p_x(x_1, x_2, ..., x_M|\theta;\lambda) \\ & = log \prod_{m=1}^{M} p_x(x_m|\theta;\lambda) \\ & = \sum_{m=1}^{M} log(\alpha p_{x,1}(x_m|\theta;\lambda) \\ & + (1-\alpha) p_{x,2}(x_m|\theta;\lambda)) \end{aligned} \tag{4.11}$$

Different non-linear optimization algorithms have been tested to find the maximum value of $p_x(x_1, x_2, ..., x_M|\theta;\lambda)$. Among optimization algorithms explored as "fminsearch", "simulated annealing" and "patternsearch", the best results, in terms of computational rapidity, have been found with "patternsearch", see section 3.3.
Since the purpose of the thesis has been only to reproduce the previous Corino model, it has only been verified the correctness of the estimation parameters compared to the provided input set without a study of statistical errors. To have a further confirm of the model, it has been checked the graphical correspondence between the simulated RR intervals histogram and the PDF built with the estimated set of parameters, see Fig. 4.7.

The result obtained is that the PDF, created by the proposed model, follows correctly the histogram.
The main evidence underlined by the PDF is the bimodality characteristic due to the presence of dual AV nodal pathways. The PDF changes its shape when the estimated parameters $\Delta\tau = (\tau_2 - \tau_1)$ (Fig. 4.8(a)), α(Fig.4.8(b)), λ(Fig.4.8(c)), τ_{p1} and τ_{p2}(Fig. 4.8(d)) are modified. Improving $\Delta\tau$ the second peak is shifted to rightside. If $\Delta\tau$ is close to 0.1 s the two peaks are hardly distinguished, whereas the α variation modifies the weight given to peaks. If α is less than 0.5, the first peak is less emphasised, otherwise there would

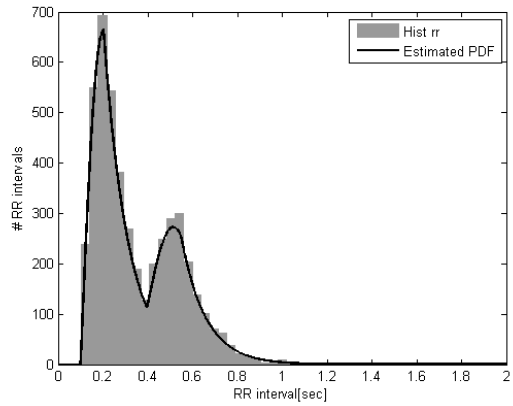

Fig. 4.7: Comparison between the RR series Histogram and the estimated PDF using λ=9.09 Hz, τ_1=0.1, τ_2=0.4, τ_{p1}=0.1, τ_{p2}=0.15,α=0.7. Simulated time registration: 28 minutes.

be the opposite behaviour with α more than 0.5. The extreme α values [0 1] produce the disappearance of one of two peaks.The AI frequency λ is proportionally correlated to peaks height. Rising λ the first peak is more affected to increase its value. The last graph is showing different τ_{p1} and τ_{p2} settings. The influence on PDF is evident by enlarging shape peaks.

4.3 Modified model

The application of the Corino et *al.* model on real data generates a high variability of the estimated parameters during the 24-h ECG recordings, in particular regarding the probability α.
The requested task has been to modify the RR series simulation through the insertion of a new input probability γ, that is considered to be closer to the electrophysiological properties of the AV node compared to the output probability α. The expected result of our work would be a more stability of the new parameter along the 24-h registration time.
The hypothesis to which for each ventricular activation the train of atrial impulses passes through the same pathway, according to α has been refused. Referring to the Fig. 4.9, each impulse has the probability γ to choose the slow pathway with shorter refractory period. The probability of conduction $\hat{\alpha}$ is estimated from the model as the ratio between the number of atrial impulses passed through the slow pathway and the total number of atrial impulses passed through either the slow pathway and the fast pathway.

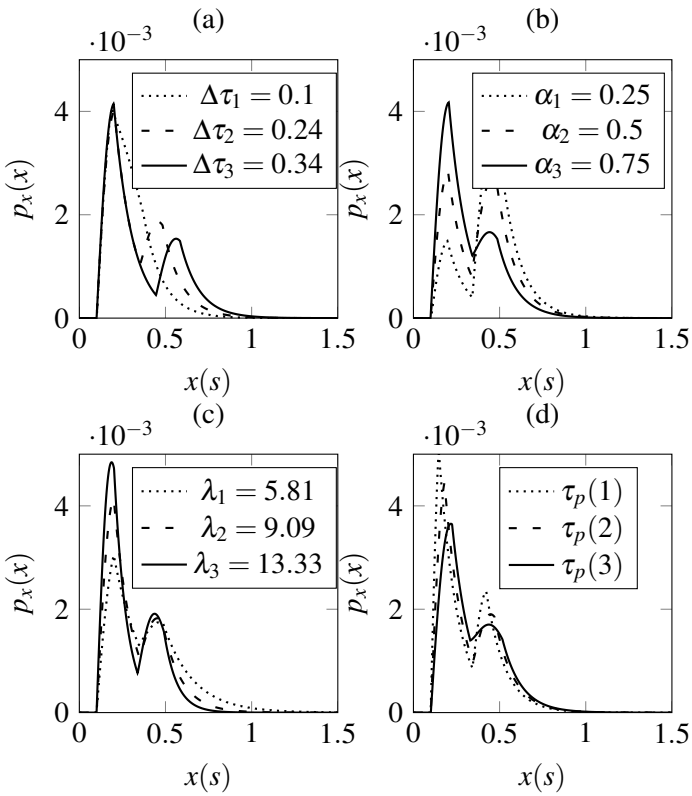

Fig. 4.8: PDF for different $\Delta\tau$(a), α(b), λ(c), τ_p(d), $\tau_{p1}(1) : \tau_{p1} = 0.05, \tau_{p2} = 0.08; \tau_{p1}(2) : \tau_{p1} = 0.08, \tau_{p2} = 0.13; \tau_{p1}(3) : \tau_{p2} = 0.12, \tau_{p2} = 0.16$. Set parameters: τ_1=0.1, τ_2=0.34,α=0.7, λ=6.25, τ_{p1}=0.1, τ_{p2}=0.15.

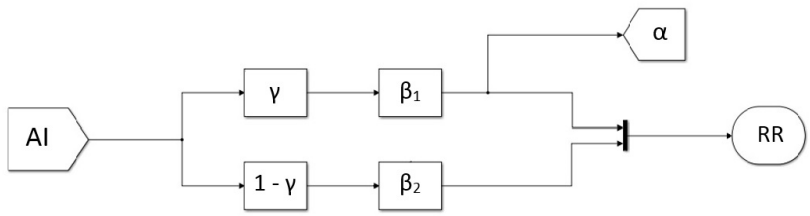

Fig. 4.9: Modified model of AV node inserting the parameter γ at the entrance to split the atrial impulses between the two pathways

The relationship existing between the input probability γ and the output probability $\hat{\alpha}$ becomes important to understand the behaviour of the model characterised by the following parameters τ_1, τ_2, τ_{p1}, τ_{p2} and γ.

Chapter 5

Results

The chapter contains at the beginning the experimental study of $\hat{\alpha}$ trend depending on the input parameters. In the next sections the discover of the experimental law is described, followed by the confirmation of the equation by studying the mean absolute error and the root mean square error. The last sections regard the inversion of the law and its application on real data.

5.1 Simulation

Different parameter settings were used to simulate RR-series, see Tab. 5.1. For each parameter setting, a 30 min RR interval series was simulated. The parameter λ was incremented with 0.5 Hz step, the step-size of $\Delta\tau$ and $\Delta\tau_p$ was 0.01 s, and the probability γ varied with 0.1 step.

Inputs	Intervals	
λ	$5-10$	[Hz]
$\Delta\tau$	$0-0.5$	[s]
$\Delta\tau_p$	$0-0.2$	[s]
γ	$0-1$	

Tab. 5.1: Set of parameters used to alpha simulation

5.1.1 Data Exploration

To study the relationship between $\hat{\alpha}$ and γ, it has been carried out:

1 $\Delta\tau = \tau_2 - \tau_1 > 0s$ is the difference between the fast pathway with longer refractory period and the slow pathway with shorter refractory period;

2 $\Delta\tau_p = \tau_{p2} - \tau_{p1}$ as difference between the two prolongations. Since the prolongation time τ_p indicates the concealed conduction phenomenon,

both conditions $\tau_{p1} < \tau_{p2}$, $\tau_{p2} < \tau_{p1}$ are possible, hence $\Delta\tau_p$ can be either $> 0s$ or $< 0s$.
The choice of the above mentioned parameters was done previously to have two parameters less, studying only the variation between the two refractory periods and the respective prolongations. Besides the two differences enhance the dependence between the two pathways. In the following paragraphs the trend of $\hat{\alpha}$ is shown depending on two parameters and fixing the other ones.

Trend of $\hat{\alpha}$ depending on γ and $\Delta\tau$

If the parameter λ is kept constant and $\Delta\tau_p = 0s$ while varying γ and $\Delta\tau$.
The mathematical function that describes the relative refractoriness of the *i*th pathway can be simplified to:

$$\beta_i(t) = \begin{cases} 0 & \text{if } 0 < t < \tau_i \\ 1 & \text{if } t \geq \tau_i \end{cases} \tag{5.1}$$

In Fig.5.1(a) each curve represents the variation of $\hat{\alpha}$ fixing $\Delta\tau$ for different γ values, while in Fig.5.1(b) the parameter $\hat{\alpha}$ has been studied depending on $\Delta\tau$ and each curve indicates a different fixed γ parameter. It is feasible to notice from the graphs:

1 $\hat{\alpha}$ increases with γ (see Fig. 5.1(a)), because increasing the probability to choose the slow pathway, a greater number of atrial impulses pass through the same one, increasing $\hat{\alpha}$;

2 increasing $\Delta\tau$ the curve will be shifted towards higher values of $\hat{\alpha}$ (Fig. 5.1(a)). The explanation is intuitive: in the time window between τ_1 and τ_2, the time-dependent refractoriness of the slow pathway $\beta_1(t) = 1$, while for the fast pathway $\beta_2(t) = 0$. Hence the atrial impulse can pass through the slow pathway, whereas it is blocked in the fast pathway. Therefore, increasing the difference $\Delta\tau$, the probability $\hat{\alpha}$ to pass through the slow pathway by the atrial impulse increases, see Fig. 5.1(b).

Regarding the Fig. 5.1(a): (1) focusing on curves with $\Delta\tau > 0s$ an exponential relationship between $\hat{\alpha}$ and γ is observed; (2) the asymptotic value 1 assumed by the parameter $\hat{\alpha}$ corresponds to the maximum value of γ.
In Fig.5.1(b) it is evident that for the initial value $\Delta\tau = 0s$ the parameter $\hat{\alpha}$ is equal to the input parameter γ, because the two functions β_1 and β_2 are characterised by the same refractoriness periods, so the probability to be

conducted by one of the two pathway is the same to the probability to choose one of them.

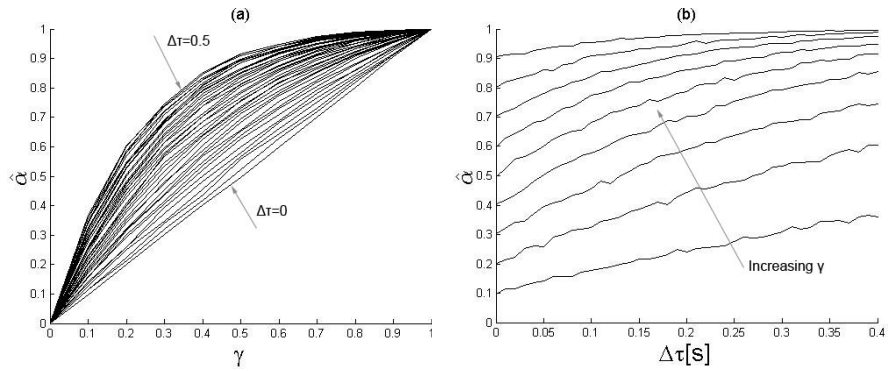

Fig. 5.1: (a)Trend of $\hat{\alpha}$ for different values of γ when $\lambda = 8.77Hz$, $\Delta\tau_p = 0s$ and $\Delta\tau = [0-0.4]s$(b) trend of $\hat{\alpha}$ for different values of $\Delta\tau$ when $\lambda = 8.77Hz$, $\Delta\tau_p = 0s$ and $\gamma = [0.1-0.9]$.

Trend of $\hat{\alpha}$ depending on γ and $\Delta\tau_p$

Establishing $\Delta\tau = 0s$ and fixing λ, $\Delta\tau_p$ was inserted (studying the condition $\tau_{p2} > \tau_{p1}$). The probability function $\beta_i(t)$ that describes the respectively refractoriness period of slow/fast pathway is thus modified:

$$\beta_i(t) = \begin{cases} 0 & \text{if } 0 < t < \tau_i \\ \dfrac{t}{\tau_{pi}} & \text{if } \tau_i \leq t < \tau_i + \tau_{pi} \\ 1 & \text{if } t \geq \tau_i + \tau_{pi} \end{cases} \tag{5.2}$$

In the Fig. 5.2(a) it is shown different curves of $\hat{\alpha}$ depending on γ for different values of $\Delta\tau_p$, while in Fig. 5.2(b) the trend of $\hat{\alpha}$ is represented varying $\Delta\tau_p$ and each trend is shown changing γ.
The observations are similar to the previous section, however in Fig.5.2(b) $\hat{\alpha}$ trend looks less influenced by the parameter $\Delta\tau_p$ compared to $\Delta\tau$. During the interval $[\tau_{p1} - \tau_{p2}]$, $\beta_1 = 1$, but β_2 is not equal to 0, so there is a probability equal to $\dfrac{t}{\tau_{pi}}$ that the atrial impulse could pass from the fast pathway. Therefore $\hat{\alpha}$ values are less altered by $\Delta\tau_p$ compared to the dependence by $\Delta\tau$.

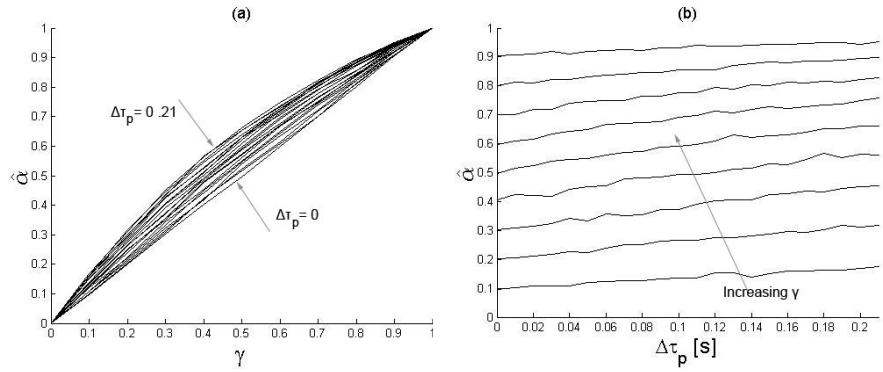

Fig. 5.2: (a)Trend of $\hat{\alpha}$ for different values of γ when $\lambda = 8.77Hz$, $\Delta\tau = 0s$ and $\Delta\tau_p = [0 - 0.21]s$(b) trend of $\hat{\alpha}$ for different values of $\Delta\tau_p$ when $\lambda = 8.77Hz$, $\Delta\tau = 0s$ and $\gamma = [0.1 - 0.9]$.

Trend of $\hat{\alpha}$ depending on γ and λ

The last analysis regards the trend between $\hat{\alpha}$ and the occurrence frequency of atrial impulses λ, setting to fixed value $\Delta\tau$ and $\Delta\tau_p = 0s$. In Fig. 5.3 $\hat{\alpha}$ increases with λ because the interval time among the atrial impulses is getting lower, so the probability of a single atrial impulse to fall in the interval $[\tau_1 - \tau_2]$ increases.

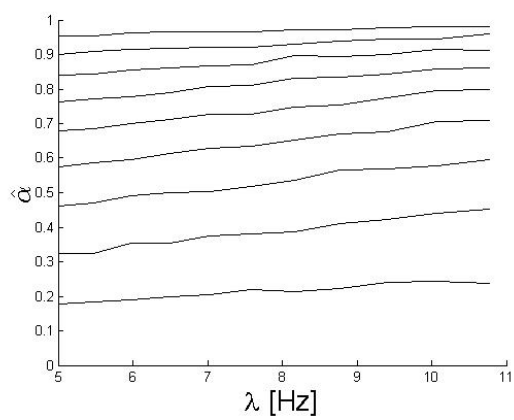

Fig. 5.3: Each curve is $\hat{\alpha}$ trend depending on λ when $\Delta\tau = 0.17s$ $\Delta\tau_p = 0s$ and $\gamma = [0.1 - 0.9]$.

5.1.2 Relationship between γ and $\hat{\alpha}$

The research of the relationship between $\widetilde{\alpha}$ and γ has been conducted by using Minimum Least Squares (MLS) algorithm, so that the whole analysis has been established following the next steps:

1. Assumption of exponential equation, which has been suggest by the different trends studied in the Sec 5.1.1;
2. Introducing limits $0 < \widetilde{\alpha} < 1$ because $\widetilde{\alpha}$ is a probability;
3. Setting bounds for the refractory periods τ_1, τ_2 and the respective prolongations τ_{p1} and τ_{p2} to the physiological range as shown in Sec 5.1;
4. Analysis of estimated coefficients furnished by MLS.

Setting $\Delta\tau_p = 0$ to simplify the study, we have suggested an exponential law for the description of the counted $\hat{\alpha}$ trend depending on the time $\Delta\tau$, see Fig. 5.1(a):

$$\widetilde{\alpha}(\Delta\tau, A, B|\Delta\tau_p = 0) = 1 - A\,e^{-B\Delta\tau} \tag{5.3}$$

where $\widetilde{\alpha}$ is the estimation of the probability $\hat{\alpha}$, while A and B represent coefficients that will be estimated by MLS. As mentioned in point 2), it has been inserted the asymptote 1 to which $\tilde{\alpha}$ can converge. The parameter A is easily

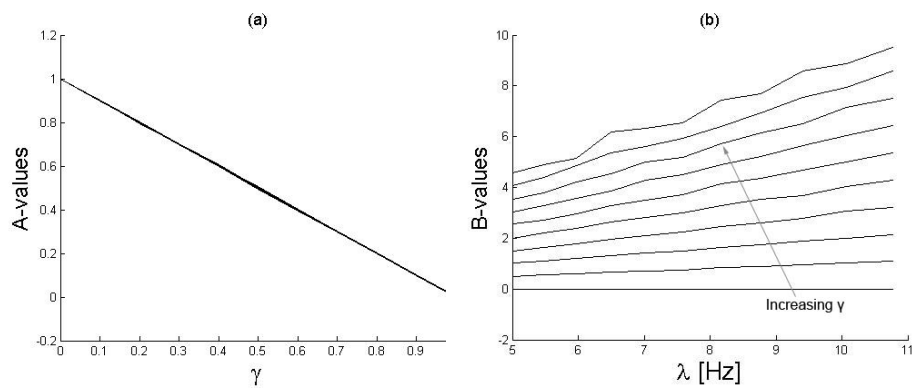

Fig. 5.4: The graphic representation of A(a)and B(b), referred to the equation 5.3, studied for different values of γ and λ, establishing $\Delta\tau_p = 0$. In (a) the curves (overlapped) have the same behaviour, setting a different λ for each curve; in (b) the curve are studied varying λ, where each curve represents a different γ value.

solved. Enforcing $\Delta\tau = 0$, it was mentioned before that the output parameter

is equal to the input one, so:

$$\widetilde{\alpha}(0) = \gamma = 1 - A;$$

$$A = 1 - \gamma$$

so the parameter A is the complementary of γ.
In Fig. 5.4(a) there is the estimation of A obtained by MLS algorithm varying the parameter γ. Observing Fig.5.4(b) the representation of B coefficient, they correspond to the product of $\lambda\gamma$. Therefore the equation will be:

$$\widetilde{\alpha}(\gamma, \Delta\tau, \lambda | \Delta\tau_p = 0) = 1 - \left[(1-\gamma)e^{-\lambda\gamma\Delta\tau}\right] \tag{5.4}$$

The following step has been to consider the elongation times ($\Delta\tau_p \neq 0$), reproducing the same procedure and setting in this case $\Delta\tau = 0$. Since the obtained trend between the counted $\hat{\alpha}$ and γ looks still an exponential (see Fig. 5.2), it has been suggested to use the same structure of the equation 5.4, changing only the exponential argument. Setting the equation:

$$\widetilde{\alpha}(\gamma, \Delta\tau_p, \lambda | \Delta\tau = 0) = 1 - \left[(1-\gamma)e^{-\lambda\gamma C\Delta\tau_p}\right] \tag{5.5}$$

C was considered as numerical constant, obtained by the average of different values of C varying γ, $\Delta\tau_p$ and λ, see Fig. 5.5. The set C is equal to 0.5.
To complete the relationship between $\widetilde{\alpha}$ and γ, the influence of the parameter $\Delta\tau_p$ was added to the refractory period $\Delta\tau$, leading to:

$$\widetilde{\alpha}(\gamma, \Delta\tau, \Delta\tau_p, \lambda) = 1 - \left[(1-\gamma)e^{-\lambda\gamma\left(\Delta\tau + \frac{\Delta\tau_p}{2}\right)}\right] \tag{5.6}$$

5.1.3 Simulation Results

Recalling the relationship between $\tilde{\alpha}$ and γ:

$$\tilde{\alpha} = 1 - \left[(1-\gamma)e^{-\lambda\gamma\left(\Delta\tau + \frac{\Delta\tau_p}{2}\right)}\right]$$

Figures 5.6 and 5.7 show the comparison between the derived probability of $\tilde{\alpha}$ obtained using above equation and the actual $\hat{\alpha}$ obtained in the simulations, as a function of $\Delta\tau$ and $\Delta\tau_p$, respectively. It can be noted that the actual trend of $\hat{\alpha}$ follows the derived $\tilde{\alpha}$

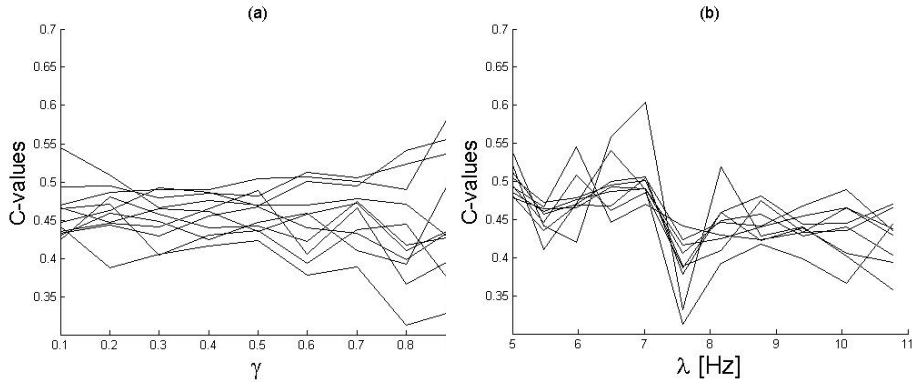

Fig. 5.5: The graphic representation of C depending of γ (a) and λ (b), referred to the equation 5.5, studied for different values of γ and λ, establishing $\Delta\tau = 0$. Both curves in (a) and (b) have the same random behaviour; in (a) each curve represents a different λ; in (b) each curve represents a different γ

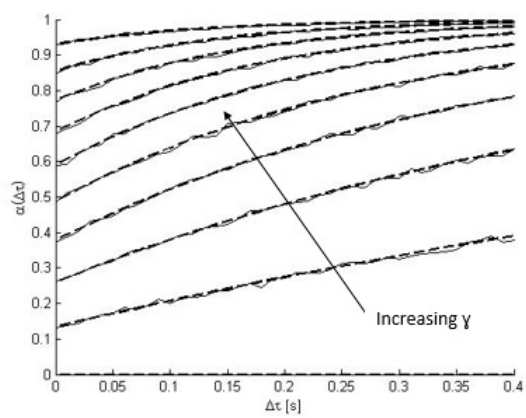

Fig. 5.6: Trends of the derived $\tilde{\alpha}$ (dashed lines) and actual $\hat{\alpha}$ (solid lines) depending on the difference between the two prolongation times ($\Delta\tau_p$). Each curve corresponds to a different value of γ that was varied from 0.1 to 0.9.

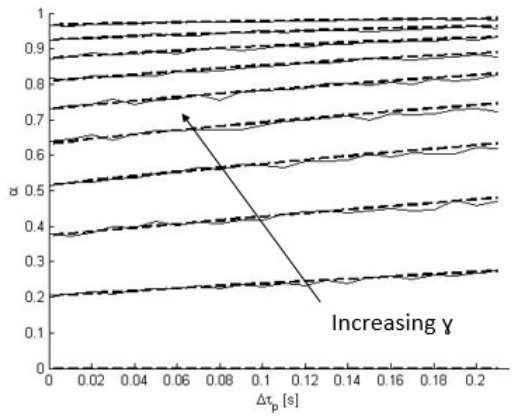

Fig. 5.7: Trends of the derived $\tilde{\alpha}$ (dashed lines) and actual $\hat{\alpha}$ (solid lines) depending of the difference between the two refractory periods ($\Delta\tau$). Each curve corresponds to a different value of γ that was varied from 0.1 to 0.9.

The mean absolute error (MAE, Eq. 5.7) and the RMSE (Root Mean Square Error, Eq. 5.8) were calculated to confirm our result, which are shown in Tab. 5.2. We used both in order to diagnose the variation in the errors in a set of estimations. Indeed, MAE is an average magnitude without considering their direction, evaluating the accuracy of the measurement, unlike RMSE is a quadratic scoring rule which measures the average magnitude of the error. Since the errors are squared before they are averaged, the RMSE gives a relatively high weight to large errors. This means the RMSE is most useful when large errors are particularly undesirable.

$$MAE = \frac{\sum_{i=1}^{m} |\hat{\alpha}_i - \tilde{\alpha}_i|}{m} \tag{5.7}$$

$$RMSE = \sqrt{\frac{\sum_{i=1}^{m} (\hat{\alpha}_i - \tilde{\alpha}_i)^2}{m}} \tag{5.8}$$

Below are shown two global index of errors

$$\bar{MAE} = 0.0038 \pm 8.2023 * 10^{-4}$$

$$\bar{RMSE} = 0.0159 \pm 0.0087$$

γ	*MAE*	*RMSE*
0.0	0.0029 ± 0.0005	0.0000 ± 0.00000
0.1	0.0033 ± 0.0005	0.0422 ± 0.00752
0.2	0.0031 ± 0.0006	0.0493 ± 0.00958
0.3	0.0033 ± 0.0007	0.0487 ± 0.00930
0.4	0.0035 ± 0.0007	0.0451 ± 0.00850
0.5	0.0047 ± 0.0008	0.0397 ± 0.0069
0.6	0.0038 ± 0.0008	0.0328 ± 0.0049
0.7	0.0038 ± 0.0009	0.0257 ± 0.0009
0.8	0.0045 ± 0.0010	0.0186 ± 0.0018
0.9	0.0045 ± 0.0011	0.0111 ± 0.0006
1.0	0.0045 ± 0.0013	0.0000 ± 0.0000

Tab. 5.2: Absolute error and RMSE between the $\tilde{\alpha}$ obtained using Eq. 5.6 and the actual value $\hat{\alpha}$.

5.1.4 Inversion

Since the purpose of the thesis is to calculate the parameter γ, it is necessary to invert the equation 5.6 in order to study γ depending on the parameters $[\Delta\tau; \Delta\tau_p; \lambda; \alpha]$ properly estimated through the Corino model, described in Sec 4.2, on dataset of patients affected to AF.
In order to invert, it is necessary to refer to the Lambert Function, defined in Sec 3.4 as the multivalued inverse of the function:

$$y = f(W) = W(x)e^{W(x)} \tag{5.9}$$

The branch considered of the Lambert function in this study is the *principal branch* ($W_0(x)$) for which $W(x) \geq -1$. To invert Eq. 5.6 it is fundamental arriving to the simplified form 5.9.
Assuming:

$$z = 1 - \gamma; \Delta T = \Delta\tau + \frac{\Delta\tau_p}{2}$$

the equation will be:

$$\widetilde{\alpha} = 1 - ze^{(-\lambda(1-z)\Delta T)} \tag{5.10}$$

Bringing the parameters non-dependent from z to the left side of the equation:

$$\widetilde{\alpha}' = ze^{(\lambda z \Delta T)}$$

where $\widetilde{\alpha}' = (1-\widetilde{\alpha})e^{(\lambda \Delta T)}$. Changing the base $b = e^{(\lambda \Delta T)}$ it is possible to arrive to the compact form similar to the (1.2):

$$\widetilde{\alpha}' = zb^z \tag{5.11}$$

Using the Lambert function property described in the article [42]:

$$y = W(x)b^{W(x)}; W(x) = \frac{W(x\log(b))}{\log(b)} \tag{5.12}$$

the final equation is:

$$\gamma = 1 - \frac{W((1-\widetilde{\alpha})\lambda \Delta T e^{(\lambda \Delta T)})}{\lambda \Delta T} \tag{5.13}$$

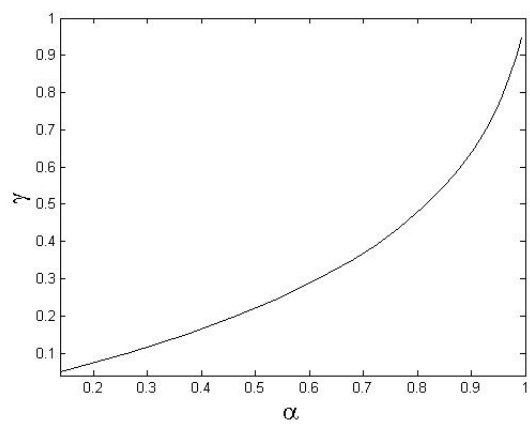

Fig. 5.8: Derived γ depending of $\hat{\alpha}$, keeping fixed $\Delta\tau = 0.2s$, $\Delta\tau_p = 0.07s$, $\lambda = 8.57Hz$

5.2 Real data

Data collected in the RATe control in Atrial Fibrillation (RATAF) study were analyzed in this work. The RATAF study was a prospective, randomized, investigator-blind, crossover study designed to compare four drug regimens

Variable	Value
Gender (male/female)	42/18
Age (years)	71 ± 9
AP duration (months)	$11(2-121)$
BMI	27 ± 4
Hypertension	25

Tab. 5.3: Demographic characteristics and cardiovascular history in the study population

(metoprolol, diltiazem, verapamil, and carvedilol) used to reduce the ventricular heart rate in patients with permanent AF. Each drug was given for more than three weeks to ensure an adequate period of washout of the previous treatment and steady-state plasma concentrations. Before starting the first treatment and at the last day of each of the 4 treatment periods, 24-h Holter recordings were made. The regional ethics committee and the Norwegian medicines agency approved the study, registered at www.clinicaltrials.gov (clinical trial no. NCT00313157) and conducted in accordance with the Helsinki Declaration. Each patient provided written informed consent before any study-related procedures were performed. The clinical characteristics of the patients are shown in Table 5.3. Data analysis was conducted on those patients which recordings have sufficient quality along the 24h. Therefore, the analysis was carried out on 31 patients, containing 155 recordings.

Starting by the following formula:

$$\gamma = 1 - \frac{W((1-\hat{\alpha})\lambda\Delta T \exp(\lambda\Delta T))}{\lambda\Delta T}$$

The probability of γ has been calculated applying the above formula on estimations previously realized by Corino model, so that it was possible a comparison between α and γ probabilities have been compared.

5.2.1 Real data results

The first part of the analysis has regarded the calculation of the mean and standard deviation values of α and γ, respectively σ_α and σ_γ. It has been found that σ_γ is resulted lower than σ_α in 58% of the analysed recordings. It is important to have an understanding of the values as a whole, hence it has

been calculated the mean values assumed respectively by α and γ.

$$\begin{aligned} \bar{\sigma_\alpha} &= 0.1857 \\ \bar{\sigma_\gamma} &= 0.1813 \end{aligned} .$$

In order to assess the difference between α and γ, it has been carried out t-test on σ_γ and σ_α for all recordings, which has confirmed the non-significant difference between α and γ. Indeed, the σ_γ presents approximately the same value of σ_α. It is now interesting to show some example which enhances the difference between α and γ and behaviour. For this purpose will be exposed two patients. The Figs. 5.9 and 5.10 show as γ gives a better result in terms

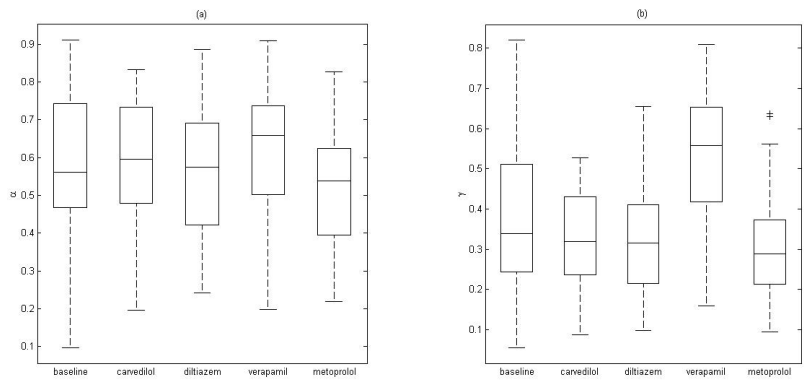

Fig. 5.9: Patient 1 : comparison α (a) and γ (b) for each treatment

of interquartile range, and confirm the usual lower values of γ, according to Eq. 5.6. The two boxplots show on right the probability of α while on the left the probability of γ. Deepening the analysis, the superimposition between α, estimated by the Corino model, and the derived γ (Figs.5.11 and 5.12) shows an expected results, according to the α and γ standard deviations. Indeed, the two behaviours have almost the same trend, γ follows α. This similar tendency between α and γ is explained mainly by the presence of a small $\Delta\tau$, indeed if $\Delta\tau \approx 0$ and $\Delta\tau_p \approx 0$, then $\alpha = \gamma$. Substantially γ trend is characterised by a lower value, which is explainable observing the Fig. 5.8 that show the tendency of γ to have a smaller than α. This is due to atrial impulses enter preferentially into the slow pathway, which is characterised by lower refractory period facilitating the passing of atrial impulses into slow pathway, increasing α, see Fig. 4.9. Instead, referring to Eq. 5.5, $\Delta\tau_p$ value

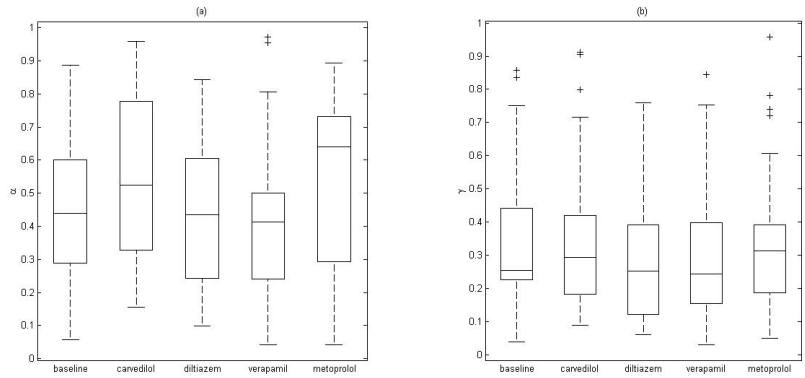

Fig. 5.10: Patient 2 : comparison α (a) and γ (b) for each treatment

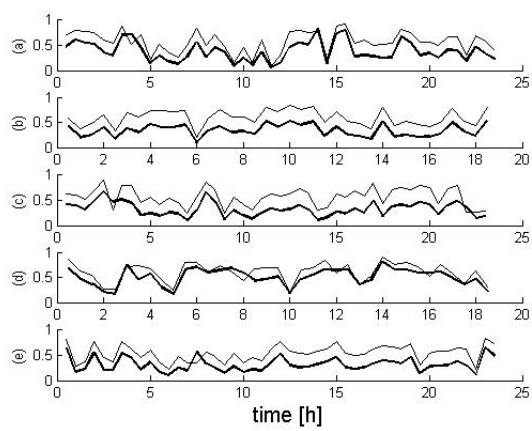

Fig. 5.11: Patient 1: Superimposition of α (solid line) and γ (thick line) during baseline (a), and Metoprolol (b), Diliziasem (c), Verapamil (d), Carvedilol (e) treatments

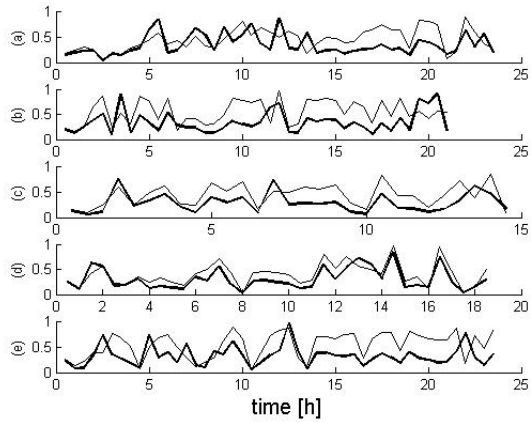

Fig. 5.12: Patient 2: Superimposition of α (solid line) and γ (thick line) during baseline (a), and Metoprolol (b), Diliziasem (c), Verapamil (d), Carvedilol (e) treatments

is weighted by a constant C equals to $1/2$, which prevents an exponential increasing too quick of γ. Hence, C coefficient prevents an overestimation of γ. However, analysing the real data the difference $\Delta\tau_p$ is not contained in the simulated interval $(0-0.2$ sec), that it means C-value may have a different value. It is noticeable that in some sample γ assumes an higher amplitude of α, especially observing the trend of τ_{p1} and τ_{p2} in both Fig.s 5.13 and 5.14. This phenomenon is observable in 5.14, referring to the prolongations. Indeed interval by interval, the difference $\Delta\tau_p$ may reach values close or higher than 0.5 Sec Hence, increasing of $\Delta\tau_p$ may lead to a constant $C \neq 0.5$.

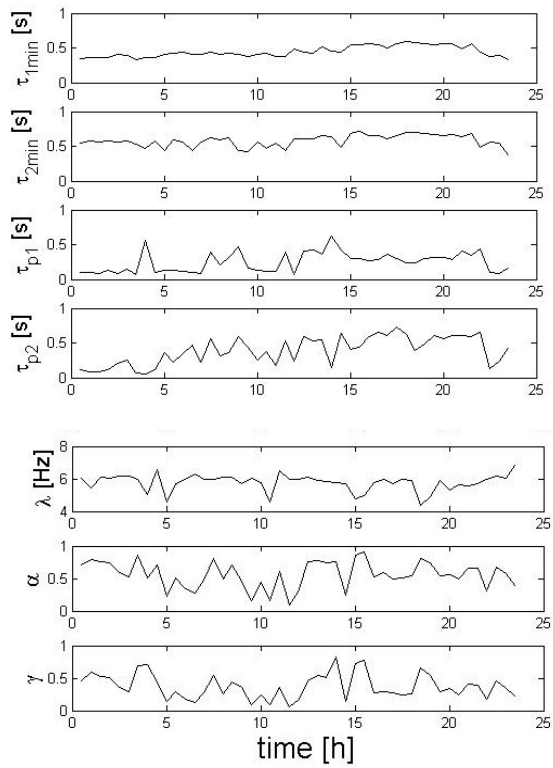

Fig. 5.13: Patient 1: Comparison along the 24h recording of all estimated parameters by Corino model and derived γ during baseline

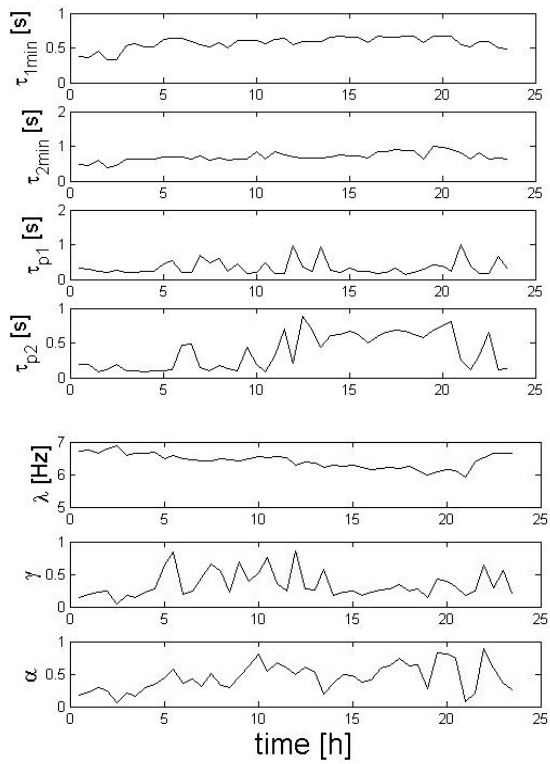

Fig. 5.14: Patient 2: Comparison along the 24h recording of all estimated parameters by Corino model and derived γ during baseline

Chapter 6

Discussions

The result of the present thesis has been the research of the relationship between $\tilde{\alpha}$ and γ that fits the experimental trend. The correctness of the law is proved by the study of MAE and RMSE, calculated between the actual $\hat{\alpha}$ and the derived $\tilde{\alpha}$, that reach the order of magnitude of $10^{-}3$, see Tab. 5.2. In the investigation of the law, the only parameter that has been not found completely stable is the parameter C, see Sec 5.1.2, discovered time-dependent from $\Delta\tau_p$. To fix this variability, the parameter C has been calculated as the average of different C coefficients varying the parameters $\Delta\tau_p$ and λ. To improve the accuracy of the estimation it has been imposed $\Delta\tau_p < 0.2s$, bound physiologically accepted. The result obtained is: $C = 0.5 \pm 0.05$; anyhow it has been accepted by the low errors obtained in $\tilde{\alpha}$. We propose in the future to improve the parameter C, understanding better its dependence from the variability $\Delta\tau_p$.
We have suggested a partial explanation of the equation, studying the case of $\Delta\tau_p = 0$. The model, in this case, is represented by the step function, see Eq. 5.1, that receives in input a Poisson process. Focusing on the step response along the fast pathway, it is feasible to set the differential equation of the variation of the probability $\tilde{\alpha}^*$ (complementary of the probability $\tilde{\alpha}$) depending on the variation time $\Delta\tau$. The integration of the proposed equation can lead to the Eq. 5.4 described in Sec 5.1.1. However, there are some assumptions that are not yet well explained. We do not know the correlation between the Poisson process given as input, and the model described by a step, therefore the response is not fully explained.
The analytically approach (Lambert function) used for the inversion of the equation between α and γ lets to avoid a numerical approximation, it means that the error committed on the measure of simulated $\hat{\alpha}$ is relatively small.

The hypothesis of the thesis regards the assumption that the parameter γ, since it is closer to the physiological properties of the AV node, should be more stable than the estimated α. However, the results on the real data show

that there is not a statistical significance between the standard deviation of γ and α, therefore the hypothesis could not be coherent. We suppose that the introduction of the new parameter γ has led to redefine the Corino model, compromising the application of the estimated parameters on the relationship $\alpha - \gamma$.

Regarding the implementation of the previous model, it has been introduced two restrictions, so that α is constrained in a range between 0 and 1, and τ_1 cannot be larger than τ_2, since the ML estimation of all parameters may generate unphysiological values. The use of Simulated Annealing was abandoned in favor of Pattern Search, computationally faster. In this study Matlab's default features are used, except for the *CompleteSearch* and *MeshRotate* set both 'on'. They respectively evaluate values around the current iterate (to find a better solution) and do not rotate the mesh before declaring a point to be optimum (avoiding complementary estimations).
Moreover, it has been noticed a high variability of the estimated parameters that can be visible in Fig. 5.13 that has many causes. The first one is implied on the acquisition of the ECG signal. Since the registration lasts 24-h, the signal can be affected by patient muscular activity that will affect the signal. Moreover, the parameter λ is largely influenced by the noise, because its estimation derives from the atrial activity that is lower in magnitude compared to the ventricular activity. Lastly, the model is highly sensitive to the estimation of τ_1. Because of ectopic beats, or generic noise, it is possible the generation of RR intervals clearly lower than RR intervals expected during AF. The result is a wrong estimation of τ_1 that brings to underestimate τ_2 and to overestimate the respective prolongations τ_{p1} and τ_{p2}.

About our opinion the estimation of the parameters by MLE is not suitable with the new version of Corino model, therefore we suggest to change, in future applications, the estimation method in order to have a one-to-one correspondence with the simulated parameters.
We are still convinced that the parameter γ can be less influenced by variability compared to the parameter $\tilde{\alpha}$. Because the former is an input parameter that cannot be affected by the refractoriness periods of dual AV node pathways as it happens to the output parameter $\tilde{\alpha}$.
Regarding the mathematical explanation of the equation, we suggest to study in detail the step response when a statistical process is inserted as input, to confirm the exponential trend that we have found in experimentally way.

Chapter 7

Conclusion

This study presents a statistical method for a quantitative analysis of AF. A previous model has been implemented initially , accomplishing all characteristic such as dual nodal pathways, concealed conduction and relative refractoriness taken into account. These aspects are modeled and estimated as the probability of the atrial signal to pass through the slow pathway, the difference in refractory period between the two pathways and the maximum prolongation. The simulation has been improved introducing a new parameter that represents the probability of an impulse choosing either one of the two pathways.

To test its accuracy and precision the mean absolute error (MAE) and root mean square error (RMSE) for different γ's has been calculate . Obtaining, $MAE = (3,8 \pm 0.82023) \times 10^{-3}$ and $RMSE = 0.0159 \pm 0.0087$, calculated as average among all errors.

Moreover, the relationship on dataset has been tested, 24-h Holter recordings were made. The results showed that the standard deviation of introduced parameter presents a greater stability in 58% of recordings. It has been carried out a t-test on the two standard deviations that enhances a not significant difference.

This study indicates that the relationship opens a new approach for the study of AF. There are certain aspects of the relationship that need improvements, e.g. a more robust C coefficient for weighing the difference of the maximum prolongations.

Bibliography

[1] World Health Organization Study: Atrial Fibrillation is a Growing Global Health Concern. *World Health Organization Study: Atrial fibrillation is a growing global health concern*. 2013. URL: https://www.cedars-sinai.edu/About-Us/News/News-Releases-2013/World-Health-Organization-Study-Atrial-Fibrillation-is-a-Growing-Global-Health-Concern.aspx.

[2] Ronald D. Berger Richard J. Cohen and Theodore E. Dushane. "A quantitative model from the ventricular response during atrial fibrillation". In: *IEEE Transactions on Biomedical Engineering* vol 12 (1983), pp. 769–781.

[3] V. Lang J. Lian D. Müssig. "computer modeling of ventricular rhythm during atrial fibrillation and ventricular pacing". In: *IEEE Transactions on Biomedical Engineering* vol 53 (1993), pp. 1512–1520.

[4] Luca T. Mainardi Valentina D.A. Corino Frida Sandberg and Leif Sörmo. "An atrioventricular node model for analysis of ventricular response during atrial fibrillation". In: *IEEE Trans. Biomed. Eng.* vol 58 (2011), pp. 3386–3395.

[5] A.J. Hill and P.A. Iaizzo. *Handbook of cardiac anatomy, physiology and devices*. Springer, 2009.

[6] J.G. Widdicombe A.C. Guyton. *Respiratory Physiology*. University Park Press, 1974.

[7] OpenStax College. In: *Micrograph*. Regents of University of Michigan Medical School, 2012.

[8] D. Prutchi and M. Norris. *Design and development of medical electronic instrumentation - PROPER UNSIGNED*. Wiley, 2005.

[9] Mark R. Boyett Natalie J. Chandelr Robert H. Anderson Joseph and Halina Dobrzyski. "The anatomy of the cardiac conduction system". In: *Wiley-Liss, Inc.* vol 22 (2009), pp. 99–113.

[10] P. Atkins J. de Paula. *Physical chemistry for the life sciences*. W. H. Freeman Publishers, 2006.

[11] D. E. Goldaman. “Potential, impedence, and Rectification in membrane”. In: *The Journal of General Physiology* (1943), pp. 37–60.

[12] N. Richard Fogoros. *Electrophysiologic testing*. Wiley, 2012.

[13] Leif Sörmo and Pablo Laguna. *Bioelectrical signal processing in cardiac and neurological applications*. Elsevier Academic press, 2005.

[14] M. Funk E. S. Kaufman M. W. Krucoff M. M. Laks P. W MacFarlene C. Sommargreen S. Swiryn G. F. van Hare B. J. Drew R. M. Califf. “Practice standards for electrocardioversion”. In: *Circulation* vol 110 (2004), pp. 2721–2746.

[15] Bax J Crijns H Camm J Diener HC Goette A Hindricks G Hohnloser S Kappenberger L Kuck KH Lip GY Olsson B Meinertz T Priori S Ravens U Steinbeck G Svernhage E Tijssen J Vincent A Breithardt G. Kirchhof P. Auricchio A. “Outcome parameters for trials in atrial fibrillation: executive summary”. In: *Eur Heart Journual* vol 28 (2007), pp. 2803–2817.

[16] URL: `http://www.doctortipster.com/3683-atrial-fibrillation-causes-diagnosis-and-treatment.html`.

[17] Richard Adamec Jan Adamec. *ECG holter*. Springer, 2008.

[18] The task force for the management of atrial fibrillation of the European Society of Cardiology (ESC). “Guidelines for the management of atrial fibrillation”. In: *European Heart Journal* vol 31 (2010), pp. 2369–2429.

[19] Leif Sörmo Luca Mainardi and Sergio Ceutti. *Understanding atrial fibrillation*. Morgan and Claypool Publishers, 2008.

[20] P. Rossi. “Strategie a confronto nel Trattamento della Fibrillazione Atriale”. In: *CARDIOLOGY SCIENCE* vol 6 (2008), pp. 129–136.

[21] I. Contrafatto. *Electical Cardioversion*. URL: `http://www.ablazione.org/terapie/cardioversione-elettrica/`.

[22] V. Williams. “Classifying antiarrhythmic actions: by facts or speculation.” In: *US National Library of Medicine National Institutes of Health* vol 11 (1992), pp. 964–77.

[23] V. Williams. “A classification of antiarrhythmic actions reassessed after a decade of new drugs.” In: *US National Library of Medicine National Institutes of Health* vol 4 (1984), pp. 129–47.

[24] M. Dohnal S.B. Olsson N. Cai and K.K. Talwar. “Noninvasive support for and characterization of multiple intranodal pathways in patients with mitral valve disease and atrial fibrillation”. In: *European Heart Journal* vol 7 (1986), pp. 320–333.

[25] Ho S. Y. Andersoon R. H. “The architecture of sinus node, the atrioventricular conduction axis, and the internodal atrial myocardium”. In: *Journal of Cardiovascular Electrophysiol* vol 9 (1998), pp. 1233–1248.

[26] Paul A. Iaizzo. *Handbook of cardiac anatomy, physiology, and devices*. Humana Press, 2005.

[27] J.B. Preston G.K. Moe and H. Burlington. “Hysiologic evidence for a dual A-V transmission system”. In: *Circ.Res.* vol 4 (1956), pp. 357–375.

[28] Todor N. Mazgalev and Patrick J. Tchou. “Surface potential from the region of atrioventricular node and their relation to dual pathway electrophysiology”. In: *Journal of American Hearth Association* vol 101 (2000), pp. 2110–2117.

[29] J. T. Vermeulen A. F.M. Moorman P. Loh B. Thibault J. Vermeulen A. E. Becker M. J. Janse M. A. McGuire J. M.T. de Bakker. “Atrioventricular junctional tissue discrepancy between histological and electrophysiological characteristics”. In: *Circulation* vol 94 (1996), pp. 571–577.

[30] J. J. Langberg. “Radiofrequency catheter ablation of AV nodal reentry: The anterior approach”. In: *Circulation* vol 87 (1993), pp. 1551–1556.

[31] R. Langerdof. “Concealed A-V conduction: The effect blocked impulses on the formation and conduction of subsequent impulses”. In: *American Heart Journal* vol 35 (1948), pp. 542–552.

[32] de Mello WC Hoffman BF P. de Carvalho A. “Hoffman BF: Electrical activity of the atrio-ventricular node”. In: *The Specialized Tissues of the Heart* (1961), pp. 143–158.

[33] J. Myung. “Tutorial on maximum likelihood estimation.” In: *Journal of Mathematical Psycology* vol 47 (2002), pp. 90–100.

[34] D. McFadden W. K. Newey. *Handbook of Econometrics*. Elsevier, 1986. Chap. Large sample estimation and hypothesis thesting - 36.

[35] Harald Cramer. *Mathematical methods of statistics*. Princeton University Press, 1999.

[36] Stefen Lauritzen. *Sufciency and Unbiased Estimation*. University of Oxford, 2004.

[37] URL: http://ashakhov.wordpress.com/2011/01/27/simulated-annealing/.

[38] J. Tsitsiklis D. Bertsimas. "Simulated Annealing". In: *Statistical Science* vol 8 (1993), pp. 10–15.

[39] Robert Michael Lewis Elizabeth D. Dolan and Virginia Torczon. "On the local convergence of pattern search". In: *Journal Optim* (2001), pp. 567–583.

[40] URL: http://www.wikipedia.com.

[41] D. E. G. Hare D. J. Jeffrey R. M. Corless G.H.Gonnet and D. E. Knuth. "On the Lambert W function". In: (2001).

[42] Citizendium. *Lambert W function*. 2011. URL: http://en.citizendium.org/wiki/Lambert_W_function.

[43] P. Pagao L. Glass L. Mangin A. Vinet. "Effects of antiarrhythmic drug therapy on atrioventricular nodl function during atrial fibrillation in humans". In: *The European Society of Cardiology* vol 7 (1993), S71–S82.

[44] Katarina In de Betou Jessica Palmqvist. "Modeling of the atrioventricular node during atrial nibrillation to non-invasively monitor drug effects". Master thesis. Lund University, 2013.